Plant Physiology and Biochemistry 238 (2026) 111698

Contents lists available at ScienceDirect

Plant Physiology and Biochemistry

journal homepage: www.elsevier.com/locate/plaphy

Surface functionalization of polystyrene nanoparticles modulates nanoparticle-induced phytotoxicity in *Chlorella vulgaris*

Bruno Komazec [a], Biljana Balen [a], Željka Vidaković-Cifrek [a], Petra Cvjetko [a], Nino Dimitrov [b], Petra Peharec Štefanić [a,*]

[a] Department of Biology, Faculty of Science, University of Zagreb, Horvatovac 102a, Zagreb, HR-10000, Croatia
[b] Croatian Institute of Public Health, Rockefellerova 7, Zagreb, HR-10000, Croatia

ARTICLE INFO

Keywords:
Nanoplastics
Cell association
Oxidative stress
Photosynthetic performance
Ultrastructural alterations

ABSTRACT

Polystyrene nanoparticles (NPs) are increasingly released into aquatic systems, but how surface formulations shape their interactions with primary producers remains insufficiently understood. We examined the effects of nominally non-functionalized polystyrene NPs (PS-NPs) and amino- (PS-NH_2-NPs) or carboxyl-functionalized NPs (PS-COOH-NPs) on *Chlorella vulgaris* after short-term 72 h exposure to a comparative high concentration (40 mg L^{-1}). All polystyrene NPs remained stable in the culture medium and were detected in EPS-associated and cell-associated fractions, with stronger relative retention of PS-NPs and PS-NH_2-NPs than PS-COOH-NPs. Because Py-GC-MS data were qualitative and relative/semi-quantitative, cell-associated signals were interpreted as retention rather than direct evidence of intracellular uptake. All NPs induced ultrastructural alterations, including plasmolysis and thylakoid disorganization, without substantially affecting growth or cell viability. PS-NPs did not increase detectable ROS at the 72 h endpoint but caused lipid, protein and DNA damage. PS-NH_2-NPs increased H_2O_2 and lipid peroxidation and enhanced pigment accumulation, whereas PS-COOH-NPs showed the most pronounced total ROS response and protein oxidation. Antioxidant responses were characterized mainly by peroxidase activation and depletion of non-enzymatic antioxidants, reflecting redox imbalance. All NPs reduced oxygen evolution at growth light intensity, although unchanged F_v/F_m and increased PI_{abs} did not indicate impairment of PSII functionality. Overall, commercial surface functionalization modulated NP retention and phytotoxic responses in *C. vulgaris*, highlighting the need to consider NP surface properties and exposure context in nanoplastic ecotoxicology.

1. Introduction

With the development of societys, plastics have become one of the most widely used materials, mainly due to their thermoplasticity, i.e. their ability to deform when heated, which makes them useful in various industries (Jin et al., 2019). They belong to the group of synthetic polymers, and since their invention in 1907, plastic production has increased significantly, from 2 million tons in the middle of the last century (Nayanathara Thathsarani Pilapitiya and Ratnayake, 2024) to 464 million tons in 2020, while 884 million tons of plastic per year are forecast for 2050 (Dokl et al., 2024). The Organisation for Economic Co-operation and Development (OECD) reported that 353 million tons of plastic entered the environment in 2019, with projections indicating an increase to approximately 1.014 billion tons annually by 2060 (OECD, 2022), posing a serious ecological threat. Plastic is not biodegradable and therefore remains in the environment for a long period of time. In addition, under the influence of various environmental conditions, e.g. increased heat, UV radiation and/or mechanical stress, plastic breaks down into smaller pieces, such as microplastics (MPs) and nanoplastics (NPs), which can be even more hazardous. Plastics consist of different types of polymers, of which polystyrene, polyethylene terephthalate, polypropylene and polyvinyl chloride are the most common (Taudul et al., 2024).

Among synthetic polymers, polystyrene is recognized as a highly persistent environmental contaminant occurring in aquatic as well as terrestrial ecosystems (Kaur et al., 2022). It is produced by the polymerization of styrene monomers and mainly used for its thermoplasticity, durability and transparency. It is found in a variety of everyday products, including toys, toothbrushes, disposable plates and cups, as well as in medical and food industry products due to its low

* Corresponding author.
E-mail address: petra.peharec.stefanic@biol.pmf.unizg.hr (P. Peharec Štefanić).

https://doi.org/10.1016/j.plaphy.2026.111698
Received 8 June 2026; Received in revised form 3 August 2026; Accepted 28 August 2026
Available online 31 August 2026

biodegradability (Loos et al., 2014). Polystyrene NPs have high reactivity and are therefore frequently used as biosensors (Velev and Kaler, 1999), for biomolecule purification (Cortés et al., 2020) and for drug delivery (Loos et al., 2014). Functionalization of their surfaces, often with amino and carboxyl groups, further improves their properties, including stability and specificity in biological fluids (Jiang and Thayumanavan, 2005; Loos et al., 2014). Due to the increasing industrial production and use of NPs in general, polystyrene NPs are being released into the environment in ever-increasing quantities, with aquatic ecosystems emerging as key accumulation sites (Turan et al., 2019), where they pose potential risks to important organisms such as autotrophic protists, especially algae, which play a crucial role in oxygen production (Field et al., 1998).

Among autotrophic protists, the alga *Chlorella vulgaris* stands out as a model organism due to its versatility, ease of cultivation and potential for various applications in biotechnology (de Abreu et al., 2014). In addition, *C. vulgaris* is frequently used in ecotoxicological studies, as it is a sensitive, readily available and well-studied aquatic organism that serves as a reliable indicator of environmental stress (Li et al., 2023a; Saxena et al., 2021). Its sensitivity to various pollutants, along with its adaptability to diverse environments, supports its use as a model organism for assessing toxicity in aquatic ecosystems (Aly et al., 2024). Of particular interest is a mucous layer called extracellular polymeric substances (EPS), a mixture of complex organic polymers and smaller amounts of proteins, lipids and nucleic acids (Babiak and Krzemińska, 2021), which is secreted by the algae into their environment. EPS plays a crucial role in various functions, including protection from harsh conditions by forming a barrier around the *C. vulgaris* cells and shielding them from environmental stressors such as extreme temperatures, salinity and desiccation (Liu et al., 2025).

Previous research indicates that plastic NPs can be toxic to green freshwater algae by impairing their growth, photosynthesis and overall physiology (reviewed in (Yang et al., 2024)). Mechanisms of toxicity include (i) induction of oxidative stress by overproduction of reactive oxygen species (ROS) and potential damage to cellular components (Natarajan et al., 2022), (ii) physical damage, as NPs can adhere to algal cells and disrupt the cell membrane (Parsai et al., 2022), (iii) reduction in nutrient uptake, which affects algal growth and metabolism (Hazeem et al., 2020), and (iv) a shading effect, which limits light penetration and reduces photosynthetic efficiency (Hund-Rinke et al., 2020; Zhao et al., 2019). The effects can vary depending on factors such as particle size, surface properties, concentration, and the specific type of plastic (Nolte et al., 2017). Recent studies on *C. vulgaris* further show that the toxicity of amino-functionalized polystyrene NPs can be strongly modified by co-contaminants and natural organic matter, with humic acid affecting eco-corona formation, zeta potential (ζ potential) dynamics and heteroaggregation between algal cells and PS-NH_2 particles (Khoshnamvand et al., 2024a, 2024b). Although plastic NPs have lower phytotoxicity compared to metal NPs, their slow biodegradability raises concerns about possible long-term consequences of chronic exposure (Awet et al., 2018).

Among the various characteristics of NPs, surface properties largely determine their reactivity and potential adverse effects. Therefore, this study focused on non-functionalized polystyrene NPs (PS-NPs) and polystyrene NPs functionalized with amino (PS-NH2-NPs) or carboxyl (PS-COOH-NPs) groups. The green alga *Chlorella vulgaris* was selected as the test organism to compare the effects of these nanoparticles under standardized short-term exposure conditions, focusing on NP stability, EPS- and cell-associated retention, oxidative stress responses, photosynthetic performance, and ultrastructural alterations. By combining these complementary levels of analysis, we aimed to identify response patterns dependent on surface functionalization or formulation rather than to establish complete dose-response or time-dependent toxicity profiles.

2. Materials and methods

Unless otherwise specified, all reagents used in this study were supplied by Sigma-Aldrich (St. Louis, MO, USA).

2.1. Polystyrene NPs

For this study, commercially available, nominally non-functionalized polystyrene NPs (PS-NPs), with amino groups (PS-NH_2-NPs) and with carboxyl groups (PS-COOH-NPs), each with a diameter of 50 nm, were used as aqueous suspensions. PS-NPs and PS-COOH-NPs, with a concentration of 2.7% (w/v), were purchased from Polysciences Europe GmbH (Hirschberg an der Bergstrasse, Germany), while PS-NH_2-NPs, with a concentration of 1.0% (w/v), were obtained from Lab261 (Palo Alto, CA, USA). According to manufacturer-provided information, PS-NPs were supplied as Polybead® microspheres in aqueous suspension with minimal surfactant in the final preparation and with a slight anionic charge attributed to sulfate ester groups. PS-COOH-NPs were supplied as carboxylated polystyrene particles in aqueous suspension, whereas PS-NH_2-NPs were supplied as a 1% solid suspension in deionized water containing a small amount of surfactant and 2 mM sodium azide as an antimicrobial agent. Quantitative functional group densities were not provided by the manufacturers. Therefore, the terms PS-NPs, PS-NH_2-NPs and PS-COOH-NPs refer to the nominal manufacturer-declared surface formulations. The available manufacturer-provided information is summarized in Table S1.

To visualize all types of polystyrene NPs, transmission electron microscopy (TEM) was used. In brief, 2 μL of each NPs suspension was placed on a 100-mesh Formvar®/copper TEM grid. After a 5-min period, any remaining suspension was removed, and the grid was allowed to air dry. The NPs were then visualized with a TF20 monochromatic microscope (FEI Tecnai G2, FEI, USA) at 200 kV equipped with a Schottky cathode. Four replicates (n = 4) were visualized for each stock suspension.

To determine the size of NPs in each stock suspension, the dynamic light scattering (DLS) was performed using a NanoBrook 90Plus instrument (Brookhaven Instruments, Holtsville, NY, USA) equipped with a red laser (660 nm) and measuring the intensity of scattered light at an angle of 180°. The data were analyzed using the Zeta Plus 5.71 program (Brookhaven Instruments, Holtsville, NY, USA), and the hydrodynamic diameters (d_H) were determined from the particle volume size distribution. The results are given as the means of 6 measurements ± standard error. The polydispersity index (PDI) was also recorded from DLS analysis (Table S1).

To determine the charge of the NPs in each stock suspension, ζ potential was measured by electrophoretic light scattering (ELS) using capillary cells on a NanoBrook 90Plus device. The ζ potentials were calculated using the Smoluchowski equation in the Zeta Plus 5.71 program, and the results are presented as the means of five measurements ± standard error.

2.2. Algal culture and exposure to polystyrene NPs

The freshwater alga *C. vulgaris* strain SAG 211-11b used in this study was obtained from the Culture Collection of Algae at Göttingen University (Experimentelle Phykologie und Sammlung von Algenkulturen (EPSAG), Georg-August-Universität, Göttingen, Germany). *C. vulgaris* was cultured in sterile liquid BBM medium (Bischoff and Bold, 1963) on an orbital shaker under long-day conditions (16 h of light, 8 h of darkness) at a temperature of 24 °C and a light intensity of 80 μmol $_{photons}$ m^{-2} s^{-1}.

The cell culture of *C. vulgaris* with an initial concentration of 1×10^5 cells mL^{-1} was prepared in 200 mL of sterile BBM medium in Erlenmeyer flasks. The algae were grown for 4 days under the above-mentioned conditions, reaching a concentration of 1×10^6 cells mL^{-1} in the exponential growth phase, and were then exposed to individual

treatments with all polystyrene NPs at a final concentration of 40 mg L^{-1} for 72 h. The control sample consisted of a cell culture to which no NPs were added. The concentration of 40 mg L^{-1} was selected as a comparative high-exposure concentration to enable direct comparison of surface-functionalization-dependent effects among PS-NPs, PS-NH_2-NPs and PS-COOH-NPs under identical exposure conditions. Each biological replicate consisted of an independently grown and treated algal culture maintained in a separate Erlenmeyer flask containing 200 mL of cell suspension. The exposure experiment was performed twice independently. In both independent experimental runs, six independently grown and treated algal cultures were prepared per treatment group, including the control, PS-NPs, PS-NH_2-NPs and PS-COOH-NPs. Thus, unless otherwise stated, endpoint analyses were based on 12 biological replicates per treatment. When technical measurements were performed within a biological replicate, these values were averaged prior to statistical analysis, and the independent algal culture was used as the experimental unit.

Cell density was determined immediately before NP exposure and after 72 h of exposure using a LUNA-II automated cell counter (Logos Biosystems, Anyang, Republic of Korea). The average specific growth rate during the exposure period was calculated for each biological replicate according to the equation $\mu = [\ln(N_{72h}) - \ln(N_0)]/t$, where N_0 and N_{72h} represent cell density immediately before exposure and after 72 h of exposure, respectively, and t represents exposure duration in days. Growth inhibition based on the average specific growth rate (I_r, %) was calculated according to OECD Test No. 201 (OECD, 2026), using the equation $I_r = [(\mu_c - \mu_t)/\mu_c] \times 100$, where μ_c represents the mean average specific growth rate of the control group and μ_t represents the mean average specific growth rate of the corresponding NP-treated group.

Cell membrane integrity was additionally assessed by propidium iodide (PI) staining and flow cytometry. After 72 h of exposure, *C. vulgaris* cells were stained with PI at a final concentration of 1 μg mL^{-1} for 5 min in the dark and analyzed using a BD FACSVerse™ flow cytometer (BD Biosciences, Piscataway, NJ, USA) equipped with a 488 nm laser. A total of 100,000 events per sample were acquired. PI-positive events were considered cells with compromised membrane integrity.

2.3. Stability of polystyrene NPs in the exposure medium

Prior to algal exposure, we measured changes in the size and charge for each type of polystyrene NPs at the concentration of 40 mg L^{-1} in BBM medium after 1, 2, 3, 4, 5, 24, 48 and 72 h using DLS and ELS methods on a NanoBrook 90Plus instrument. d_H and PDI were determined by DLS, while ζ potential and instrument-recorded conductance were obtained during ELS measurements. The ζ potential was calculated by the instrument software from electrophoretic mobility using the Smoluchowski equation; however, raw electrophoretic mobility values were not exported from the stored measurement reports. Results are presented as the means of 6 measurements ± standard error for d_H and as the means of five measurements ± standard error for ζ potential. PDI and conductance are shown as instrument-recorded values. The pH of BBM medium and NP suspensions in BBM medium was measured immediately after preparation and after 72 h of incubation. The nominal ionic strength of BBM medium was calculated from its chemical composition.

2.4. Fractionation and relative analysis of polystyrene NPs associated with algal cells and the EPS layer

To assess the presence and relative retention of polystyrene NPs in the EPS-associated and the cell-associated fractions, pyrolytic gas chromatography coupled with mass spectrometry (Py-GC-MS) was used (Okoffo and Thomas, 2024). After 72 h of treatment, the cell suspension was centrifuged at 3500 × g for 5 min at room temperature (RT). The resulting precipitate was resuspended in 10 mL of buffer [9 mM NaCl, 1 mM KCl, 4 mM $NaH_2PO_4 \times H_2O$, 2 mM $Na_2HPO_4 \times 12H_2O$ (pH 7.0)] with the addition of 5 g of Amberlite HPR1100 ion-exchange resin to separate the EPS surface layer from the cells. After incubation at 4 °C for 2 h, the homogenate was centrifuged at 4500 × g at 4 °C for 30 min. The pellet, representing the cell-associated fraction after EPS removal, was lyophilized. This fraction may include both internalized NPs and particles strongly attached to the cell wall or membrane that were not removed during the fractionation procedure. Therefore, it was interpreted as a cell-associated fraction and not as direct evidence of intracellular uptake. The supernatant was then placed into clean vials, combined with 10 mL of cold acetone, and incubated overnight at −20 °C. The samples were then centrifuged at 4500 × g at 4 °C for 30 min and the resulting precipitate, representing the EPS surface layer fraction, was lyophilized.

The prepared samples, including algal cells, the EPS fraction, and 2 μL of each stock NPs suspension (100 mg L^{-1}), were placed separately in deactivated stainless-steel containers. The samples were then pyrolyzed in a pyrolyzer (EGA/Py3030D, Frontier Laboratories Europe, Essen, Germany) at a furnace temperature of 600 °C with an interface temperature of 300 °C, equipped with an automatic sampling device (AS-1020E, Frontier Laboratories Ltd., Koriyama, Japan). The pyrolyzer was connected to the split/split injection port of a gas chromatograph coupled to a mass spectrometer (GC-MS) (GCMS-QP2010 Plus, Shimadzu Europa GmbH, Duisburg, Germany). The GC injection port was maintained at 300 °C and connected to the quadrupole mass detector via a separation column (Ultra ALLOY ± 5, 30 m × 0.25 mm, Frontier Laboratories Ltd., Koriyama, Japan) and a vent-free GC/MS adapter (Frontier Laboratories Ltd., Koriyama, Japan). The column oven was programmed from 40 °C to 320 °C at a heating rate of 20 °C min^{-1}, with helium as the carrier gas at a flow rate of 0.87 mL min^{-1} in pressure control mode. The GC/MS interface was set to 300 °C, and the injection was performed in split mode with a split ratio of 1:16. The mass spectrometer operated with an ion source temperature of 250 °C, electron ionization at 70 eV, and a scan range of m/z 29-350. Analysis of pyrolysis products revealed polystyrene monomers, dimers, and trimers. However, signals at retention times corresponding to monomers and dimers were also observed in control algal samples, making these peaks non-specific for PS-NPs under the applied conditions. In contrast, the styrene trimer peak was detected only in NP-treated samples and was absent from blank and algal control samples. Therefore, polystyrene was identified based on the styrene trimer peak detected at a retention time of 17.3 min. Peak identity was supported by matching the corresponding mass spectrum with the F-Search all in one data search libraries (ver. 3.6) (Frontier Laboratories Ltd., Koriyama, Japan), by comparison with the analyzed PS-NP, PS-NH_2-NP and PS-COOH-NP stock suspensions, and by the absence of the styrene trimer signal in untreated control fractions. Because calibration curves, recovery rates, LOD/LOQ values, internal standard correction, and matrix-spiked controls were not available for the EPS-associated and cell-associated fractions, Py-GC-MS data were interpreted qualitatively and relative/semi-quantitatively. Therefore, relative differences among treatments and fractions were evaluated based on styrene trimer peak intensities and were not interpreted as absolute quantitative measurements of PS-NP uptake or intracellular accumulation.

2.5. Oxidative stress parameters

2.5.1. Protein extraction

Total soluble proteins were isolated from cell suspensions after exposure to all types of polystyrene NPs at a final concentration of 40 mg L^{-1} for 72 h, as well as from control cell cultures. In brief, a total volume of 200 mL of cell suspension was centrifuged at 3500 × g at RT for 5 min. The cell pellet was washed three times with ultrapure water (ion-free Milli-Q water, 18.2 MΩ-cm resistivity, Millipore Sigma, Burlington, MA, USA), with centrifugation repeated under identical settings after each wash. After washing, the cell pellet was resuspended in 500 μL of 0.1 M potassium phosphate buffer (pH 7.0) with the addition of 0.08 g silica beads (425-600 μm) and homogenized three times for 4 min at a

frequency of 30 Hz using the Retsch MM200 homogenizer (Retsch, Haan, Germany). Between each homogenization step, the carrier with the samples was cooled to 4 °C for 1 min. After homogenization, the resulting homogenates were centrifuged at 20,000 × g and 4 °C for 15 min. The supernatant was then centrifuged again under identical settings in clean tubes for 45 min. Protein concentrations in the samples were measured using the Bradford assay (Bradford, 1976), with bovine serum albumin (BSA) used as the reference standard. The samples obtained were utilized for the analysis of antioxidant enzyme activities and protein carbonyl content.

2.5.2. ROS determination

Two fluorescent probes, dihydroethidium (DHE), specific for superoxide radicals, and 2,7-dichlorodihydrofluorescein diacetate (H_2DCFDA), which detects overall ROS, were used to analyze the ROS content in *C. vulgaris* cells following previously described protocols (Hazeem et al., 2020; Ng and Ooi, 2021). Cells exposed to 40 mg L^{-1} polystyrene NPs were incubated separately with the probes in a microtiter plate at a final probe concentration of 45 μM for 30 min in the dark. Fluorescence was recorded with excitation/emission settings of 520/600 nm for DHE and 504/550 nm for H_2DCFDA using a GloMax microplate reader (Promega, Madison, WI, USA). For DHE and H_2DCFDA assays, each biological replicate was measured in three technical wells, and technical well readings were averaged before normalization and statistical analysis. Data were normalized to cell counts and expressed relative to control cells.

Hydrogen peroxide (H_2O_2) content was determined using a modified protocol based on Mátai (2017). 200 mL of the cell suspension was centrifuged (3500 × g, 5 min, RT), washed three times, and homogenized in cold 70% ethanol with silica beads. Homogenates were centrifuged (15,000 × g, 10 min, 4 °C), and 100 μL of the supernatant was mixed with xylenol orange/Fe(II) reagent [124 μM xylenol orange sodium salt, 99 mM sorbitol, 0.248 mM ammonium iron (II) sulfate] for 15 min in the dark. Absorbance at 560 nm was used to calculate H_2O_2 concentrations from a standard curve, expressed as μmol H_2O_2 $(10^6 \text{ cells})^{-1}$.

2.5.3. Damage to biomolecules

Lipid peroxidation was assessed via malondialdehyde (MDA) content following a modified protocol Heath and Packer (1968) described in detail in our previous study (Komazec et al., 2023). A 200 mL cell suspension was centrifuged (3500 × g, 5 min, RT), washed three times, and homogenized in 0.5% thiobarbituric acid in 20% (w/v) trichloroacetic acid (TCA) (T.T.T. Ltd., Sveta Nedelja, Croatia) with silica beads. Homogenates were incubated at 95 °C for 30 min, centrifuged (14,000 × g, 30 min, 4 °C), and supernatant absorbance was measured at 532 and 600 nm. MDA content was calculated from turbidity-corrected readings and expressed as μmol $_{MDA}$ $(10^6 \text{ cells})^{-1}$.

Protein oxidation was evaluated by quantifying protein carbonyls using 2,4-dinitrophenylhydrazine (DNPH), as detailed in our earlier study (Komazec et al., 2023). Briefly, protein extracts were incubated with DNPH or acid control, precipitated with TCA, washed with ethanol/ethyl acetate, and resuspended in 6 M urea. Absorbance at 370 and 280 nm was used to determine protein carbonyl content and protein concentration, respectively, with BSA standards for calibration.

DNA damage was analyzed via the comet assay as previously described (Komazec et al., 2023). Cells were embedded in low-melting agarose on pretreated slides, lysed, subjected to electrophoresis (26 V, 300 mA, 20 min), neutralized, and stained with GelStarTM (Lonza AG, Visp, Switzerland). Nuclei were visualized with a fluorescence microscope, and % tail DNA was quantified from 100 nuclei per slide using OpenComet (Gyori et al., 2014) in ImageJ 1.53t program (National Institutes of Health, Bethesda, MD, USA). For each biological replicate, one slide was prepared and 100 randomly selected nuclei were analyzed. The median % tail DNA was calculated for each slide and used as the value for the corresponding biological replicate. Results represent means ± SE of 12 biological replicate medians per treatment.

2.5.4. Antioxidant enzyme activity

Protein extracts in 0.1 M potassium phosphate buffer were used to assay antioxidant enzyme activities via UV/Vis spectrophotometry (ATI UNICAM UV4, Cambridge, UK), as described in detail in our previous study (Komazec et al., 2023).

Pyrogallol peroxidase (PPX) activity was determined by monitoring pyrogallol oxidation in the presence of H_2O_2, with absorbance recorded at 430 nm every 15 s for 2 min (Nakano and Asada, 1981). Results are expressed as μmol $_{purpurogallin}$ min^{-1} $mg^{-1}_{protein}$.

Ascorbate peroxidase (APX) activity was measured as the decrease in absorbance at 290 nm during ascorbate oxidation, recorded every 15 s for 1 min (Nakano and Asada, 1981). Results are expressed as μmol $_{oxidized\ ascorbate}$ min^{-1} $mg^{-1}_{protein}$.

Catalase (CAT) activity was assessed by spectrophotometric measurement of H_2O_2 decomposition at 240 nm, monitored every 10 s for 1 min (Aebi, 1984). Results are expressed as μmol $_{H2O2}$ min^{-1} $mg^{-1}_{protein}$.

Superoxide dismutase (SOD) activity was determined by inhibition of nitroblue tetrazolium photoreduction at 560 nm. The reaction was initiated by riboflavin under light exposure (8 min, RT), and specific activity was calculated from a standard curve of known SOD concentrations (0.025-1 U μL^{-1}) (Beauchamp and Fridovich, 1971). Results are expressed as U $mg^{-1}_{protein}$.

2.5.5. Non-enzymatic antioxidants

Proline and glutathione (GSH/GSSG) levels were determined following the protocols described in our previous study (Komazec et al., 2023), based on modified methods from Bates et al. (1973) and Salbitani et al. (2017). Cells were centrifuged (3500 × g, 5 min, RT), washed, and extracted in 3% sulfosalicylic acid using bead-assisted homogenization. The homogenates were then centrifuged (10,000 × g, 15 min, 4 °C), and the resulting supernatants were used for further analyses.

Proline content was quantified via the acidic ninhydrin reaction, with absorbance recorded at 520 nm and concentrations calculated from a standard curve. Results are expressed as μmol $_{proline}$ $(10^6 \text{ cells})^{-1}$.

Reduced glutathione (GSH) was measured using the 5,5′-dithiobis(2-nitrobenzoic acid) (DTNB) assay at 412 nm, while total glutathione was determined following enzymatic reduction in the presence of NADPH and glutathione reductase. Oxidized glutathione (GSSG) was calculated as the difference between total glutathione and GSH, and cellular redox status was expressed as the ratio of GSH to GSSG.

2.6. Photosynthetic parameters

2.6.1. Content of chlorophyll a, chlorophyll b and carotenoids

Pigments were isolated from a suspension of 7.5 × 10^6 cells and quantified for chlorophyll *a* (chl *a*), chlorophyll *b* (chl *b*) and carotenoids using the extraction protocol detailed in our previous publication (Komazec et al., 2025). Briefly, cells were washed by repeated centrifugation (3500 × g, 5 min, RT) and subjected to sequential acetone extraction with bead-assisted homogenization. Combined supernatants were adjusted to 2 mL with cold 90% acetone, and pigment concentrations were calculated from absorbance readings at 470, 647, and 664 nm using established equations (Dere, 1998; Jeffrey and Humphrey, 1975). Results are expressed as μg $_{chl\ a}$ $(10^6 \text{ cells})^{-1}$, μg $_{chl\ b}$ $(10^6 \text{ cells})^{-1}$ and μg $_{carotenoids}$ $(10^6 \text{ cells})^{-1}$.

2.6.2. Photosynthetic rate

To determine oxygen evolution and uptake, 1.5 mL of the cell suspension was added to the reaction chamber of the Chlorolab 2 instrument (Hansatech Instruments Ltd, King's Lynn, UK) and the amount of oxygen was measured at 25 °C with constant stirring and increasing light intensities of 40, 80 and 120 μmol $_{photons}$ m^{-2} s^{-1}. The algal suspension was illuminated for 20 min at each light intensity and subsequently, after each illumination, maintained in darkness for 20 min.

Photosynthetic and dark respiration rates are expressed as nmol O_2 h^{-1} $(10^6$ cells$)^{-1}$ and represent means of three biological replicates ± standard error from three independent experiments.

2.6.3. Fluorescence parameters of chlorophyll a

To evaluate the maximum quantum yield of PSII photochemistry (F_v/F_m) and the performance index on an absorption basis (PI_{abs}), 3 mL of dark-adapted samples were transferred to the AquaPen device (Photon Systems Instruments, Drásov, Czech Republic), where the polyphasic increase of chl *a* fluorescence was triggered by a light pulse intensity of 1590 μmol m^{-2} s^{-1} (peak emission at 455 nm). The parameters (F_v/F_m and PI_{abs}) were recorded using software FluorPen ver. 1.1.1.3 (Photon Systems Instruments, Drásov, Czech Republic). In addition to F_v/F_m and PI_{abs}, selected JIP-test parameters, including absorption flux per active reaction center (ABS/RC), electron transport flux per active reaction center (ET_0/RC), and dissipated energy flux per active reaction center (DI_0/RC), were calculated to further assess PSII energy fluxes.

2.7. Ultrastructural analysis

Transmission electron microscopy TEM was used to assess polystyrene NPs-induced ultrastructural changes, following the protocol described in our previous study (Komazec et al., 2023). Briefly, centrifuged cells (3500 × g, 3 min) were fixed in glutaraldehyde (cacodylate buffer, pH 7.2), embedded in agarose, post-fixed with osmium tetroxide, dehydrated in ethanol, and embedded in Spurr's resin. Sections were stained with Reynolds lead citrate and UranyLess (Em-Grade.com, Mauressac, France) prior to examination at 70 kV (Morgagni 268D, FEI Europe B.V., Eindhoven, Netherlands).

2.8. Analytical interference controls

Additional analytical interference controls were performed to evaluate whether polystyrene NPs affected spectrophotometric or fluorometric assay readouts. Cell-free aged BBM medium and aged NP suspensions (40 mg L^{-1}, 72 h in BBM) were used to assess optical light attenuation and assay-specific background signals. Apparent absorbance spectra were recorded from 400 to 700 nm immediately after preparation and after 72 h of incubation using a SPECORD 50 PLUS spectrophotometer (Analytik Jena, Jena, Germany). Spectra were corrected by subtracting the corresponding BBM medium spectrum, and light attenuation was calculated as $[1 - 10^{-A}] \times 100$, where A represents the mean corrected apparent absorbance across 400-700 nm.

For photosynthetic pigment determination, aged NP suspensions were tested as acetone blanks, added to pigment extracts, or added to control algal cells before pigment extraction. For H_2O_2 determination, aged NP suspensions were tested as reagent blanks and in the presence of a 40 μM H_2O_2 spike standard. For MDA/TBARS, aged NP suspensions were tested as TBA/TCA blanks and in the presence of a 1,1,3,3-tetraethoxypropane (TEP)/MDA-equivalent spike standard. MDA/TBARS values were corrected as $A_{532} - A_{600}$. For DHE and H_2DCFDA assays, cell-free NP/probe controls and control algal cells resuspended in aged NP suspensions were analyzed, and fluorescence values were corrected by subtracting the corresponding no-probe controls. For protein carbonyl determination, aged NP suspensions were tested as blanks and in combination with control protein extracts, with values corrected using the corresponding acid controls. Recovery or relative signal values were calculated against the corresponding aged BBM controls, which were set to 100%.

Analytical interference controls were performed using six analytical replicate preparations. For DHE and H_2DCFDA controls, each analytical replicate was measured in three technical wells, whereas spectrophotometric controls were measured in duplicate. Technical readings were averaged before calculating corrected absorbance and recovery or relative fluorescence values.

2.9. Statistical analysis

For all analyses, the independently grown and treated algal culture in a separate Erlenmeyer flask was considered the biological replicate and statistical unit. When performed, technical measurements were averaged before statistical analysis. Unless otherwise stated, statistical analyses were performed using 12 biological replicates per treatment obtained from two independent exposure experiments. Endpoints with a different number of biological replicates are indicated in the corresponding method descriptions and figure legends. Data were tested for normality using the Shapiro-Wilk test and for homogeneity of variances using Levene's test. Since both assumptions were met ($p > 0.05$), differences among treatments were evaluated by one-way ANOVA followed by the Tukey's honestly significant difference (HSD) post hoc test for multiple comparisons. Differences were considered statistically significant at $p \leq 0.05$. For the comet assay, 100 nuclei were analyzed on one slide prepared from each biological replicate. The median % tail DNA was calculated for each biological replicate, and these median values were used for statistical analysis. Exploratory principal component analysis (PCA) was performed using biological replicates to integrate the measured physiological and biochemical parameters and to visualize treatment-specific response patterns after 72 h of exposure to different polystyrene NPs. Each row in the PCA input matrix represented one independently grown and treated algal culture, resulting in 48 observations in total (four treatment groups × 12 biological replicates). The PCA included oxidative stress markers, biomolecular damage parameters, antioxidant enzyme activities, non-enzymatic antioxidants, pigment content, and chlorophyll fluorescence parameters. Before performing PCA, all variables were standardized to unit variance because the measured parameters were expressed in different units and ranges. The first two principal components (PC1 and PC2) were used for graphical representation and interpretation of the overall treatment-related response patterns. PCA was used as an exploratory visualization tool and not as a confirmatory statistical test. All statistical analyses were performed using STATISTICA 14.0.0.15 (TIBCO Software, Inc., Palo Alto, CA, USA), and differences were considered statistically significant at $p \leq 0.05$.

3. Results

3.1. Properties of polystyrene NPs in stock suspensions

TEM analysis of the suspensions of PS-NPs, PS-NH_2-NPs and PS-COOH-NPs showed particles with a very regular spherical shape (Fig. 1). The diameter of PS-NPs was 49-62 nm, that of PS-NH_2-NPs was 40-52 nm, while PS-COOH-NPs had a size range of 45-55 nm. DLS analysis revealed a d_H value of 73.8 nm for PS-NPs, 62.1 nm for PS-NH_2-NPs and 63.2 nm for PS-COOH-NPs (Table S1). The corresponding PDI values were low for all stock suspensions, indicating narrow particle size distributions. The ζ potentials were 13.16, 11.83 and 12.27 mV for the suspensions of PS-NPs, PS-NH_2-NPs and PS-COOH-NPs, respectively.

3.2. Properties of polystyrene NPs in exposure medium

After adding all types of polystyrene NPs to the BBM medium, their size did not change significantly until the end of the experiment (Table S2). PDI values remained below 0.2 throughout the 72 h exposure period for all NP types, supporting the absence of pronounced aggregation in BBM medium. The d_H values at the beginning and at the end of the experiment were 70.6 and 69.8 nm for PS-NPs, 50.0 and 53.7 nm for PS-NH_2-NPs, and 55.5 and 55.4 nm for PS-COOH-NPs, respectively, confirming their stability in the BBM medium. In contrast, the analysis of the ζ potential (Table S3) showed that the addition of PS-NPs to the BBM medium led to the formation of a positive charge during the first 5 h, after which the value became negative (−36.14 mV) until the 48th hour and then positive again (25.08 mV) at the end of the experiment.

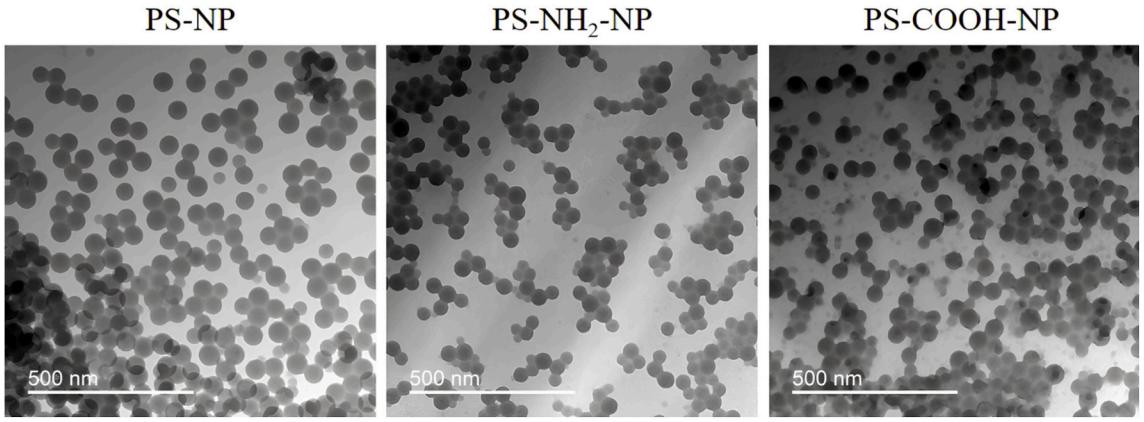

Fig. 1. Regular spherical shape of PS-NPs, PS-NH_2-NPs and PS-COOH-NPs confirmed by transmission electron microscopy (TEM). Representative images of polystyrene NPs in stock suspensions of PS-NPs, PS-NH_2-NPs and PS-COOH-NPs obtained by TEM. Four replicates (n = 4) were analyzed for each stock suspension. The scale corresponds to 500 nm.

Similarly, the addition of PS-NH_2-NPs to the BBM medium resulted in a net positive charge (17.63 mV) on the NPs surface until the 24th hour, after which the charge became negative (−16.99 mV) and remained so until the end of the experiment. A similar result was obtained with PS-COOH-NPs, where the total charge on the particle surface was positive until the end of the first day, except for the first hour when the surface charge became negative with a measured value of −29.57 mV. After 24 h, the charge remained negative until the end of the experiment, with a ζ potential value of −22.61 mV. Conductance values recorded during ELS measurements remained within a comparable range across treatments and time points (Table S3). The pH of BBM medium and NP suspensions showed only minor changes between 0 and 72 h, while the calculated nominal ionic strength of BBM medium was approximately 8.8 mM (Table S4).

3.3. Effects of polystyrene NPs on algal growth and cell viability

To determine whether the applied NP concentration affected algal growth, cell density and average specific growth rate were evaluated during the 72 h exposure period. Cell density before exposure was comparable among all groups, and no significant differences in final cell density or average specific growth rate were observed after exposure to PS-NPs, PS-NH_2-NPs or PS-COOH-NPs compared to the control (Table S5). Growth inhibition based on average specific growth rate was low in all treatments, ranging from 1.30% to 3.61%. In addition, representative PI flow cytometry plots showed a low proportion of PI-positive cells in both control and NP-treated samples, indicating that the applied NP concentration did not cause a pronounced loss of cell membrane integrity, suggesting the absence of substantial cell death (Fig. S1).

3.4. Relative retention of polystyrene NPs in cell-associated and EPS-associated fractions

Py-GC-MS analysis showed that exposure to all forms of polystyrene NPs resulted in detectable polystyrene signals in both the cell-associated fraction (Fig. 2A4, B4, C4) and the EPS-associated fraction (Fig. 2A5, B5, C5). In contrast, no styrene trimer signal was detected in the corresponding control fractions (Fig. 2A2, A3, B2, B3, C2, C3). Relative quantification of styrene trimer peaks based on peak intensities indicated that PS-NPs and PS-NH_2-NPs were retained at higher levels than PS-COOH-NPs in both fractions. In addition, ion chromatogram peak intensities were consistently higher in the EPS-associated fraction than in the cell-associated fraction after all treatments, suggesting that most polystyrene NPs were retained in the outer EPS layer, whereas only a smaller fraction remained associated with the cells after EPS removal. Because this approach was relative/semi-quantitative, these differences were interpreted as relative retention patterns rather than absolute amounts of internalized NPs.

3.5. Ultrastructural alterations

TEM analysis revealed that exposure to all types of polystyrene NPs induced plasmolysis in *C. vulgaris* cells relative to the control (Fig. 3). Treatment with PS-NPs resulted in the most severe ultrastructural alterations (Fig. 3B), including stronger plasmolysis and a more pronounced reduction in thylakoid membranes than those observed after exposure to PS-NH_2-NPs and PS-COOH-NPs, indicating pronounced destabilization of the thylakoid system.

3.6. Generation of ROS

According to the fluorescence intensities obtained with the ROS-detecting probes DHE (Fig. 4A) and H_2DCFDA (Fig. 4B), among the treatments with different types of polystyrene NPs, only exposure of algal cells to PS-COOH-NPs resulted in significantly increased values compared to the control. As for the H_2O_2 content, in addition to the treatment with PS-COOH-NPs, which gave significantly the highest value, exposure to PS-NH_2-NPs also resulted in the statistically significant increase compared to the control and to PS-NPs, although not as high as with PS-COOH-NPs (Fig. 4C).

3.7. Biomolecular damage

Analyses of biomolecular damage showed that different classes of biomolecules exhibited distinct responses to the various polystyrene NPs treatments (Fig. 5). Exposure to PS-NPs resulted in significantly increased levels of MDA, protein carbonyls, and % tail DNA compared to the control, indicating oxidative damage to lipids, proteins, and DNA, respectively. Treatment with PS-NH_2-NPs caused a similar elevation in MDA levels as observed with PS-NPs, suggesting that membrane lipids are highly susceptible to amine-functionalized PS-NPs. The genotoxic response, indicated by an increase in % tail DNA, was also present but less pronounced than in the PS-NPs treatment. As for the PS-COOH-NPs exposure, protein carbonylation levels were elevated to a degree similar to that caused by PS-NPs, suggesting protein impairment, while DNA damage remained comparable to that observed with PS-NH_2-NPs, indicating a moderate genotoxic effect.

3.8. Modulation of antioxidant enzyme activities

Different effects of the various polystyrene NPs treatments were also

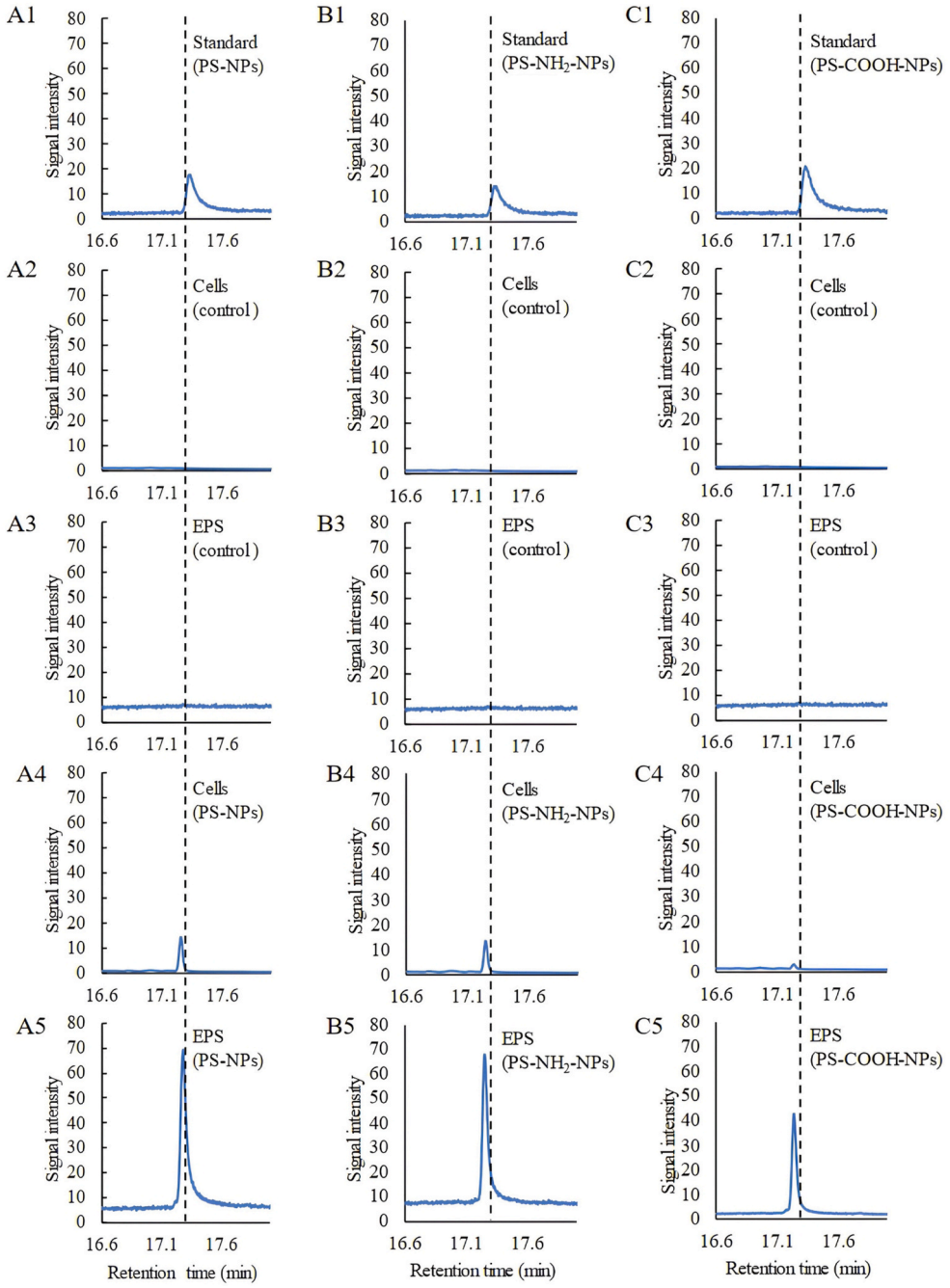

Fig. 2. PS-NPs and PS-NH_2-NPs showed stronger retention in cell-associated and EPS-associated fractions of *Chlorella vulgaris* cells than PS-COOH-NPs. Extracted ion chromatograms of styrene trimers in *C. vulgaris* control cells (A2, B2, C2) and EPS layer (A3, B3, C3), as well as in the cell-associated fraction and EPS layer after 72 h of exposure to 40 mg L^{-1} PS-NPs (A4, A5), PS-NH_2-NPs (B4, B5) and PS-COOH-NPs (C4, C5) obtained by pyrolytic gas chromatography coupled with mass spectrometry (Py-GC-MS). For each treatment applied, the pyrolysis product of stock standard suspensions of the corresponding polystyrene NPs (A1, B1, C1) is shown. Styrene trimer peak intensities were used for relative/semi-quantitative comparison of polystyrene retention among fractions and treatments. The cell-associated fraction represents material remaining with the cell fraction after EPS removal and was not interpreted as direct evidence of intracellular uptake.

evident in the modulation of the enzymatic antioxidant defense system (Fig. 6). Exposure to PS-NPs resulted in a significant upregulation of APX activity, with only a minimal, non-significant increase in PPX activity relative to the control. In contrast, treatments with both functionalized NPs led to a more pronounced activation of PPX and APX, although APX activity was significantly higher after exposure to PS-NH_2-NPs than to PS-COOH-NPs. CAT activity showed a weaker non-significant response in all treatments compared to the control, although the increase recorded with PS-NH_2-NPs was significant relative to PS-NPs. Notably, only PS-NH_2-NPs caused a significant decrease in SOD activity. Moreover, although the increase observed with PS-NPs was not significant compared to the control, it represents a significant increase in SOD activity relative to both PS-NH_2-NPs and PS-COOH-NPs, suggesting treatment-specific modulation of superoxide detoxification under these conditions.

3.9. Reduction of non-enzymatic antioxidants

The content of non-enzymatic antioxidants decreased in all treatments with polystyrene NPs compared to the control (Fig. 7). Notably,

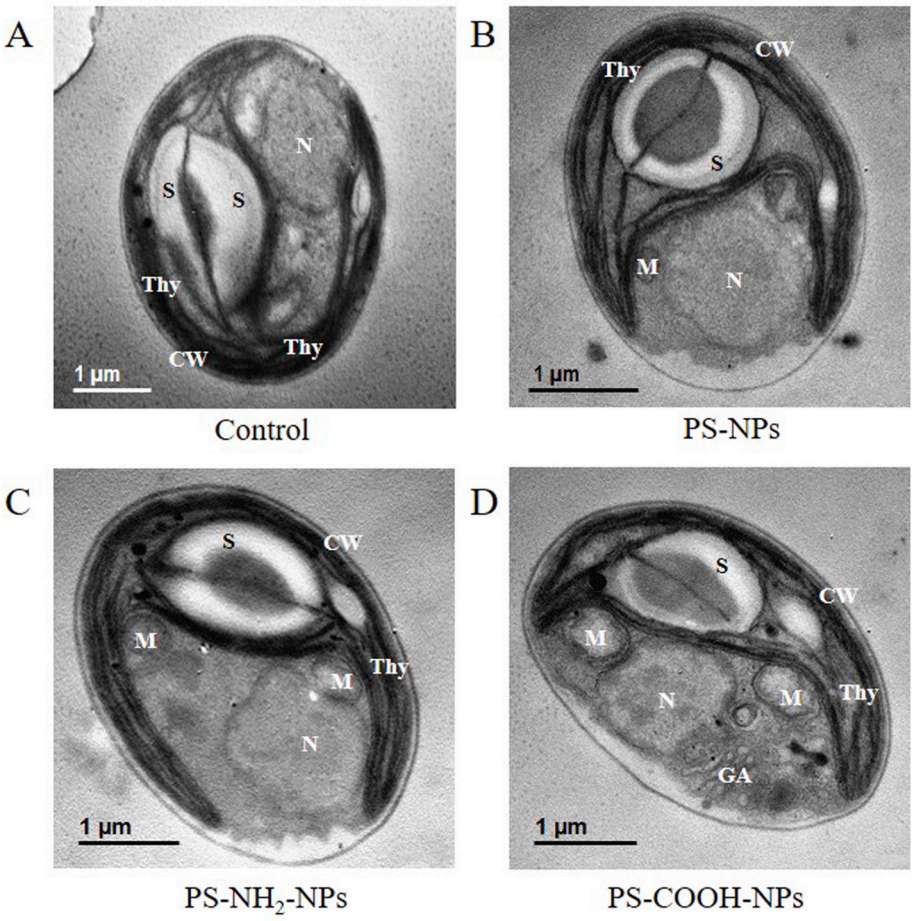

Fig. 3. All polystyrene NPs caused ultrastructural changes in *Chlorella vulgaris*. Ultrastructure of the *C. vulgaris* control cell (A) and cells after 72 h of exposure to 40 mg L^{-1} PS-NPs (B), PS-NH_2-NPs (C) and PS-COOH-NPs (D). Thy - thylakoids; S - starch; CW - cell wall; N - nucleus; M - mitochondria; GA - Golgi apparatus; red arrows indicate changes in the cell wall and membrane. The scale corresponds to 1 μm.

proline content was significantly lower in all treatments compared to the control, with the most substantial decrease following exposure to PS-NH_2-NPs, which showed significantly lower levels than the other treatments (Fig. 7A). In addition, analysis of the GSH/GSSG ratio showed a similar decrease in all treatment groups compared to the control, indicating a shift in the cellular redox balance toward a more oxidized state, characterized by decreased levels of reduced glutathione (GSH) and increased levels of its oxidized form (GSSG) (Fig. 7B).

3.10. Modulation of photosynthetic pigment composition

The tested polystyrene NPs had different effects on chl *a*, chl *b* and carotenoids content (Fig. 8). Exposure to PS-NH_2-NPs caused an overall increase in all measured photosynthetic pigments, although this increase was statistically significant only for carotenoids. The content of chl *a* and chl *b* remained comparable to the control but were significantly higher than after exposure to PS-NPs. Moreover, PS-NP treatment markedly reduced levels of chl *a* and carotenoids compared with the control, whereas PS-COOH-NPs did not cause significant changes in pigment content relative to the control.

3.11. Photosynthetic rate impairment under increased illumination intensity

Photosynthetic rate measurements showed that none of the polystyrene NPs led to statistically significant changes in oxygen under dark conditions (0 μmol photons m^{-2} s^{-1}) or at a light intensity of 40 μmol photons m^{-2} s^{-1} (Fig. 9). However, at an illumination intensity of 80 μmol photons m^{-2} s^{-1}, which corresponds to the light intensity used for algal cultivation, all NP treatments resulted in a decrease in photosynthetic rate compared to the control, with stronger inhibitory effects observed after exposure to PS-NH_2-NPs and PS-COOH-NPs. At the highest light intensity of 120 μmol photons m^{-2} s^{-1}, all NP treatments caused a comparable decrease in photosynthetic rate relative to the control.

3.12. Different effects on chlorophyll fluorescence parameters

Although F_v/F_m did not differ significantly from the control in any treatment, PS-COOH-NPs showed a significantly higher F_v/F_m value than PS-NPs (Fig. 10A). In contrast, all treatments significantly increased the PI_{abs} value compared with the control, with PS-NPs showing the smallest increase and PS-COOH-NPs yielding the highest value, which was significantly higher than that of PS-NPs (Fig. 10B). To further evaluate PSII energy fluxes, selected JIP-test parameters were analyzed (Fig. S2). ABS/RC was significantly reduced after exposure to PS-NH_2-NPs and PS-COOH-NPs compared with the control, whereas PS-NPs did not differ significantly. A similar pattern was observed for DI_0/RC, which was also significantly lower after treatment with PS-NH_2-NPs and PS-COOH-NPs. In contrast, ET_0/RC remained unchanged across all treatments.

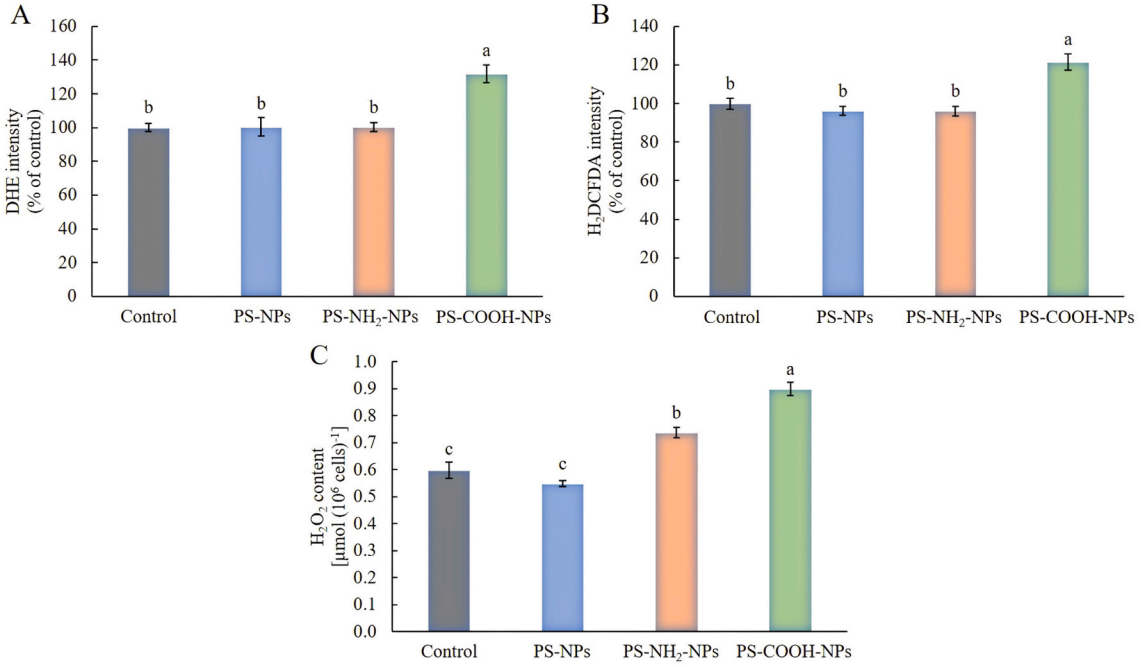

Fig. 4. The highest induction of ROS was detected after exposure of *Chlorella vulgaris* to PS-COOH-NPs. Levels of reactive oxygen species (ROS) in *C. vulgaris* control cells and cells after 72 h of exposure to 40 mg L^{-1} PS-NPs, PS-NH_2-NPs and PS-COOH-NPs. The content of total ROS was determined *in situ* using the fluorescent probes dihydroethidium (DHE) (A) and 2,7-dichlorodihydrofluorescein diacetate (H_2DCFDA) (B), while the content of hydrogen peroxide (H_2O_2) (C) was measured in cell extracts. Values represent means ± standard error of two different experiments, with 6 biological replicates each (n = 12). Treatments that differ significantly at $p \leq 0.05$ (one-way ANOVA followed by a Tukey HSD post hoc test) are indicated by different letters.

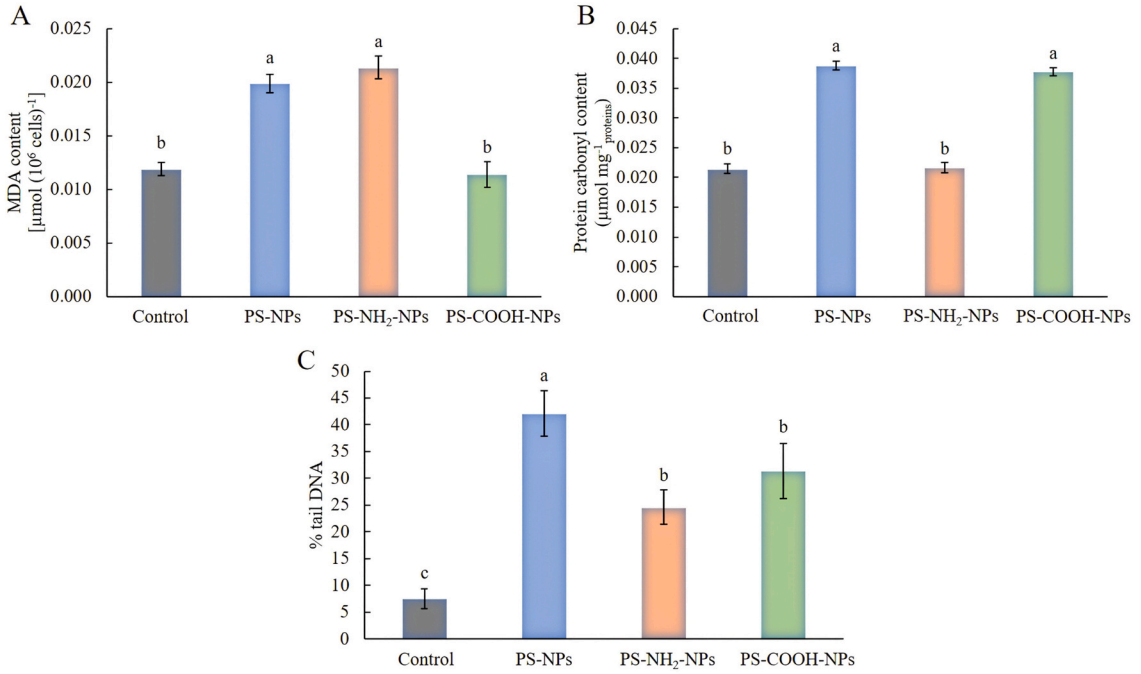

Fig. 5. Lipids, proteins, and DNA in *Chlorella vulgaris* responded differently to the various polystyrene NPs, with PS-NPs causing the most pronounced damage. Malondialdehyde (MDA) (A) and protein carbonyl (B) content and percentage of tail DNA (C) in *C. vulgaris* control cells and cells after 72 h of exposure to 40 mg L^{-1} PS-NPs, PS-NH_2-NPs and PS-COOH-NPs. Values represent means ± standard error of two different experiments, with 6 biological replicates each (n = 12). For the comet assay, one slide was prepared from each biological replicate, 100 nuclei were analyzed per slide, and the median % tail DNA value was used for statistical analysis. Treatments that differ significantly at $p \leq 0.05$ (one-way ANOVA followed by a Tukey HSD post hoc test) are indicated by different letters.

3.13. Analytical interference controls and optical light attenuation

Additional analytical interference controls showed no substantial or systematic interference of polystyrene NPs with the spectrophotometric and fluorometric assays used in this study (Table S6). Pigment recovery values in the presence of NPs ranged from 91.4% to 107.4%, while H_2O_2,

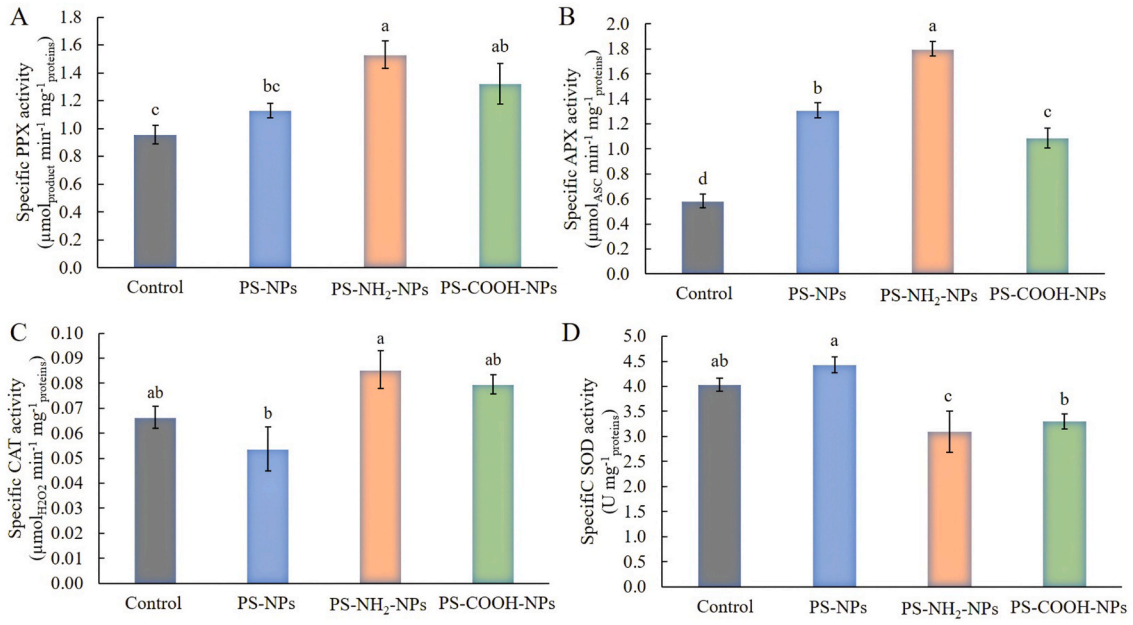

Fig. 6. Functionalized polystyrene NPs differentially modulate H_2O_2-scavenging enzymes (PPX, APX, and CAT) in *Chlorella vulgaris* compared to PS-NPs. Activities of the antioxidant enzymes pyrogallol peroxidase (PPX) (A), ascorbate peroxidase (APX) (B), catalase (CAT) (C) and superoxide dismutase (SOD) (D) in *C. vulgaris* control cells and cells after 72 h of exposure to 40 mg L^{-1} PS-NPs, PS-NH_2-NPs and PS-COOH-NPs. Values represent means ± standard error of two different experiments, with 6 biological replicates each (n = 12). Treatments that differ significantly at $p \leq 0.05$ (one-way ANOVA followed by a Tukey HSD post hoc test) are indicated by different letters.

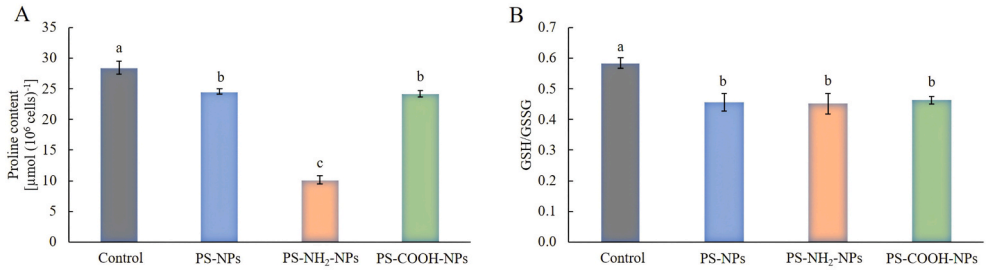

Fig. 7. The content of non-enzymatic antioxidants decreased in *Chlorella vulgaris* after treatment with all types of polystyrene NPs. Proline content (A) and the ratio of reduced and oxidized glutathione (GSH/GSSG) (B) in *C. vulgaris* control cells and cells after 72 h of exposure to 40 mg L^{-1} PS-NPs, PS-NH_2-NPs and PS-COOH-NPs. Values represent means ± standard error of two different experiments, with 6 biological replicates each (n = 12). Treatments that differ significantly at $p \leq 0.05$ (one-way ANOVA followed by a Tukey HSD post hoc test) are indicated by different letters.

MDA/TBARS and protein carbonyl recovery or relative signal values ranged from 94.4% to 105.1%. Similarly, cell-free and cell-based controls for DHE and H_2DCFDA showed relative corrected fluorescence values close to those of the corresponding aged BBM controls (Table S6). Cell-free optical measurements showed limited light attenuation for PS-NPs and PS-NH_2-NPs, whereas PS-COOH-NPs showed a moderate increase after 72 h, reaching a mean light attenuation of 7.19% across the 400-700 nm range (Fig. S3; Table S6).

3.14. Multivariate analysis

Exploratory principal component analysis provided an integrated visual overview of the physiological and biochemical responses of *C. vulgaris* to different polystyrene NPs (Fig. 11). The first two principal components explained 48.83% of the total variance, with PC1 accounting for 27.20% and PC2 for 21.63%.

The PCA score plot (Fig. 11A) revealed distinct treatment-related response patterns, particularly for the two functionalized NP treatments. Samples exposed to PS-COOH-NPs were mainly positioned in the positive PC2 region, whereas PS-NH_2-NP-treated samples shifted toward negative PC1 and negative PC2 values. Control samples and samples exposed to PS-NPs were positioned mainly on the positive side of PC1 and showed partial overlap, indicating that PS-NPs induced a less distinct overall multivariate separation than the functionalized NPs.

The corresponding loadings plot (Fig. 11B) showed that positive PC2 values were mainly associated with ROS-related parameters, including total ROS, superoxide and H_2O_2, together with protein oxidation, DNA damage, F_v/F_m and PI_{abs}. These variables were therefore more closely related to the PS-COOH-NP response profile. In contrast, negative PC1 and negative PC2 values were mainly associated with photosynthetic pigment content and lipid peroxidation, which contributed to the separation of samples exposed to PS-NH_2-NPs. Antioxidant enzyme activities, particularly APX, PPX and CAT, contributed mainly to the negative side of PC1, whereas proline content, SOD activity and glutathione content contributed to the positive side of PC1.

Overall, the exploratory PCA provided an integrated visualization of the treatment-specific responses observed in the univariate analyses. PS-NH_2-NPs were mainly associated with pigment-related adjustment and lipid peroxidation, whereas PS-COOH-NPs were more strongly associated with ROS accumulation, H_2O_2-related responses and protein oxidation. Non-functionalized PS-NPs showed a multivariate position that overlapped more with the control, consistent with a less distinct

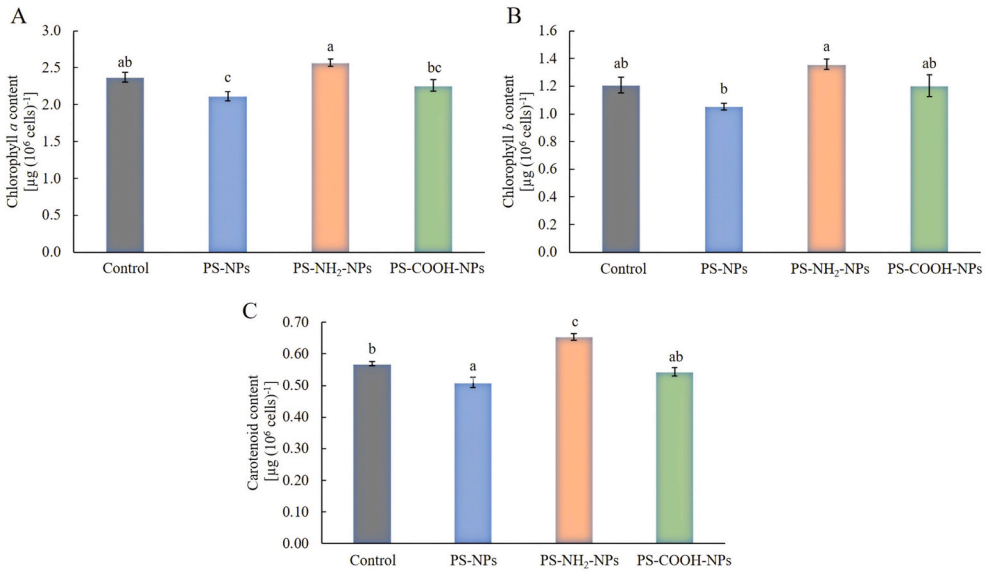

Fig. 8. PS-NPs decreased, whereas PS-NH_2-NPs tended to increase photosynthetic pigment content in *Chlorella vulgaris*. The content of chlorophyll *a* (A), chlorophyll *b* (B) and carotenoids (C) in *C. vulgaris* control cells and cells after 72 h of exposure to 40 mg L^{-1} PS-NPs, PS-NH_2-NPs and PS-COOH-NPs. Values represent means ± standard error of two different experiments, with 6 biological replicates each (n = 12). Treatments that differ significantly at $p \leq 0.05$ (one-way ANOVA followed by a Tukey HSD post hoc test) are indicated by different letters.

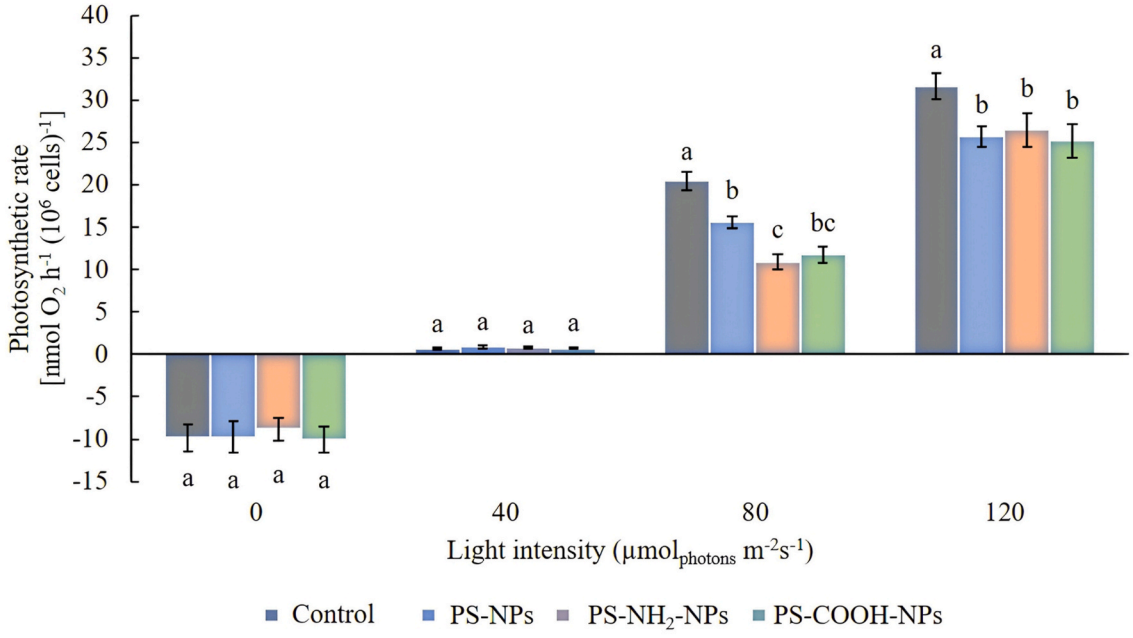

Fig. 9. All types of polystyrene NPs caused inhibition of photosynthetic rate in *Chlorella vulgaris* at illumination of 80 and 120 μmol photons m^{-2} s^{-1}. Photosynthetic rate in *C. vulgaris* control cells and cells after 72 h of exposure to 40 mg L^{-1} PS-NPs, PS-NH_2-NPs and PS-COOH-NPs at increasing values of illumination intensity (0, 40, 80 and 120 μmol photons m^{-2} s^{-1}). Values represent means ± standard error of three biological replicates. Treatments that differ significantly at $p \leq 0.05$ (one-way ANOVA followed by a Tukey HSD post hoc test) are indicated by different letters.

global response profile despite the observed biomolecular damage and photosynthetic impairment. Loading values are provided in Table S7.

4. Discussion

Polystyrene is a major contributor to the global issue of micro- and nanoplastics, as its particles are widely distributed in the environment. Their pervasive presence in aquatic ecosystems is a cause for concern, as they can accumulate in organisms and subsequently transfer to higher trophic levels (Alimi et al., 2018). Polystyrene particles have been shown to readily adsorb to organic material, including algal surfaces, facilitating their uptake into the food web and posing ecological and health risks to various organisms, including humans (Chae et al., 2018; Le Juge et al., 2023; Li et al., 2022a; Pradel et al., 2021). In this context, the exposure concentration of 40 mg L^{-1} represents an elevated experimental exposure level for inducing measurable cellular responses and enabling direct comparison among the three NP types under identical short-term exposure conditions. Given the wide variability and methodological differences in reported environmental concentrations of polystyrene particles in aquatic systems (Jachimowicz et al., 2026), this

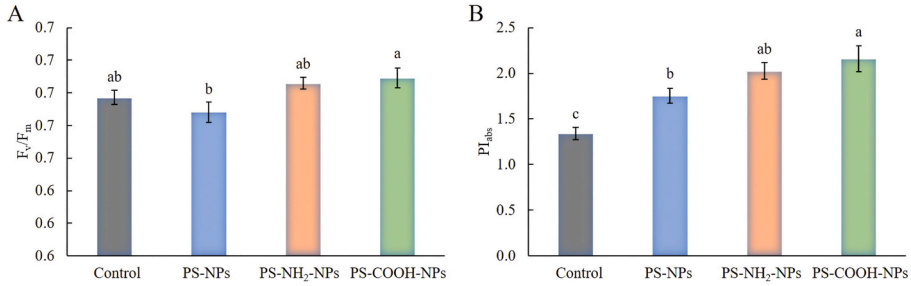

Fig. 10. All types of polystyrene NPs increased PI_{abs} without reducing F_v/F_m in *Chlorella vulgaris*. Maximum quantum yield of PSII photochemistry (F_v/F_m) (A) and performance index on absorption basis (PI_{abs}) (B) in *C. vulgaris* control cells and cells after 72 h of exposure to 40 mg L^{-1} PS-NPs, PS-NH_2-NPs and PS-COOH-NPs. Values represent means ± standard error of two different experiments, with 6 biological replicates each (n = 12). Treatments that differ significantly at $p \leq 0.05$ (one-way ANOVA followed by a Tukey HSD post hoc test) are indicated by different letters.

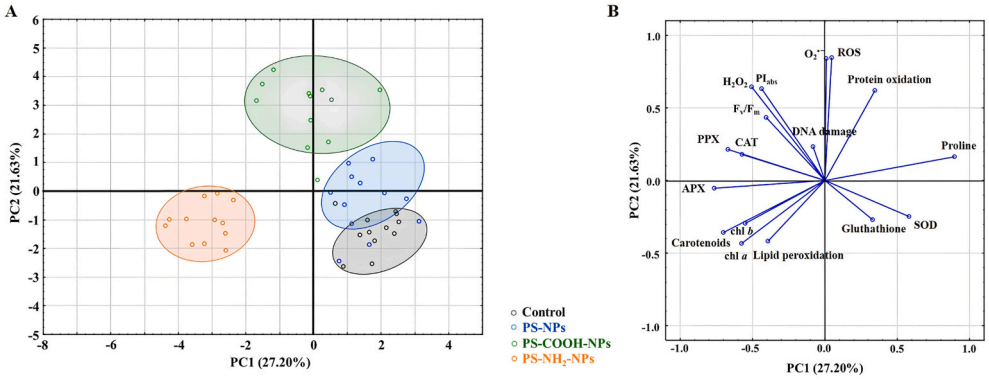

Fig. 11. Exploratory principal component analysis distinguished treatment-specific physiological and biochemical responses of *Chlorella vulgaris* to different polystyrene NPs. Exploratory principal component analysis (PCA) of physiological and biochemical parameters in *C. vulgaris* control cells and cells after 72 h of exposure to 40 mg L^{-1} PS-NPs, PS-NH_2-NPs and PS-COOH-NPs. (A) PCA score plot showing the distribution of samples according to the first two principal components, PC1 and PC2, which explained 27.20% and 21.63% of the total variance, respectively. Ellipses indicate the distribution pattern of samples within each treatment group. (B) PCA loadings plot showing the contribution of individual physiological and biochemical parameters to the observed separation of samples.

exposure scenario provides a controlled comparative framework for assessing surface-functionalization-dependent differences in NP behavior and algal responses. This framing is also supported by recent studies using substantially lower, environmentally relevant PS-NH_2 concentrations in *C. vulgaris*, which showed that NP effects can depend strongly on co-exposure conditions and on the presence of humic substances (Khoshnamvand et al., 2024a, 2024b). Therefore, the present 40 mg L^{-1} exposure should be interpreted as a comparative high-exposure scenario rather than as a direct representation of environmentally realistic NP concentrations.

In our study, *C. vulgaris* cells were exposed to both non-functionalized polystyrene NPs and NPs functionalized with specific chemical groups. Polystyrene particles are functionalized to modify their surface properties and improve their suitability for various applications, especially in biomedicine and analytical chemistry. Functionalization allows better control over the behavior of polystyrene NPs and improves their interactions with biological molecules, enabling specific targeting and enhancing their potential to act as carriers for other substances (Loos et al., 2014). Polystyrene is inherently hydrophobic, which can limit its interaction with biological systems. Functionalization with hydrophilic groups, such as the carboxyl or amino groups used in this study, can increase biocompatibility and make polystyrene NPs more suitable for biomedical applications such as drug delivery and cell culture (Gayathri et al., 2025; Loos et al., 2014). However, functionalized polystyrene particles, especially at the nano- and microscale, can exhibit varying degrees of toxicity depending on the surface modification. While polystyrene itself is generally considered relatively inert, its functionalization may introduce new properties that affect interactions with biological systems, as reported for the planktonic crustacean *Daphnia magna* (Lin et al., 2019), HepG2 human liver cells (Banerjee et al., 2022; He et al., 2020), and microbes (Zhao et al., 2024). However, studies on functionalized polystyrene nanoparticles in freshwater green algae remain scarce, with only a few reports available for *Scenedesmus obliquus* (Giri and Mukherjee, 2021; Natarajan et al., 2022) and *Pseudokirchneriella subcapitata* (Nolte et al., 2017). Importantly, very few studies have systematically compared the phytotoxic effects of differently functionalized polystyrene NPs on oxidative stress and photosynthetic performance (Zhang et al., 2022), highlighting the significance of the present investigation.

The temporal DLS analysis showed that all types of NPs maintained stable sizes in the BBM medium used for exposure. This was further supported by consistently low PDI values throughout the exposure period, indicating that pronounced aggregation did not occur under the applied BBM exposure conditions. This observation is consistent with previous findings on the stability of non-functionalized polystyrene NPs (Biba et al., 2023) and those functionalized with amino or sulfonic acid groups (Sun et al., 2020). In contrast, marked changes in surface charge (ζ potential) were observed for all NP types. Initially, all NPs exhibited a positive ζ potential, but this charge did not remain constant over time. PS-NPs showed pronounced fluctuations: their ζ potential shifted to strongly negative values after 24 h, remained relatively stable for the next 24 h and reverted to a positive charge after 72 h. The functionalized polystyrene NPs showed similar trends in surface charge dynamics, with both carboxyl- and amino-functionalized NPs maintaining a positive ζ potential for up to 48 h, after which it shifted to negative values that persisted until the end of the experiment. These differences likely reflect interactions with cations in the BBM growth medium: PS-NPs interact more readily with ions, causing faster and more frequent changes in

surface charge, whereas surface functional groups limit cation binding and enhance polystyrene nanoparticle stability (Alimi et al., 2018; Tallec et al., 2019; Yu et al., 2019; Zhang et al., 2019). The additional conductance, pH and ionic strength data further define the measurement matrix and support the interpretation that the observed ζ potential dynamics were related to interactions between NP surfaces and the ionic composition of the BBM medium. Similar matrix-dependent behavior has been reported for PS-NH_2 particles in the presence of humic acid, where sorption of humic substances and eco-corona formation shifted the ζ potential toward more negative values and reduced heteroaggregation between *C. vulgaris* cells and particles (Khoshnamvand et al., 2024a, 2024b). This supports the view that NP surface charge in algal exposure media is not a fixed particle property but a dynamic parameter shaped by the surrounding ionic and organic matrix. These findings indicate that surface functionalization/formulation plays a significant role in modulating the stability and surface charge behavior of polystyrene NPs in freshwater systems. Furthermore, the observed charge changes may modulate interactions with the cell surface, as periods of positive ζ potential could transiently favor electrostatic attraction to the negatively charged algal envelope. However, this interpretation should be considered cautiously because ζ potential values in BBM reflect the measurement matrix and may be influenced by adsorption of medium components.

The accumulation of polystyrene NPs in aquatic ecosystems, particularly at the base of the food chain, in organisms such as algae, is well documented (Chae et al., 2018). Py-GC-MS, an established technique for detecting and semi-quantitatively assessing polystyrene MPs and NPs in plant species (Biba et al., 2023; Li et al., 2021a; Taylor et al., 2020), was used in this study to evaluate the presence and relative retention of polystyrene NPs in EPS-associated and cell-associated fractions of *C. vulgaris*. The results showed that all types of polystyrene NPs were detected in the cell-associated fraction after EPS removal, while the styrene trimer signal was much stronger in the EPS-associated fraction. This suggests that most polystyrene NPs were retained within the protective EPS layer, whereas a smaller fraction remained closely associated with algal cells. However, because the Py-GC-MS data were interpreted qualitatively and relative/semi-quantitatively, the cell-associated signal should not be considered direct evidence of intracellular uptake or absolute NP accumulation. Similar observations were previously reported by Gopalakrishnan and Kashian (2022), who showed that plastic particles tend to accumulate in the EPS layer rather than in the *Chlamydomonas* cells themselves. This is probably because functional groups and long-chain molecules present in EPS form a matrix that attracts and binds plastic particles, while also promoting the formation of larger aggregates that can precipitate in the water column (Hadiyanto et al., 2025; Khatiwada et al., 2023; Nolte et al., 2017). In addition, a significantly higher and approximately equal relative polystyrene signal was observed after treatment with both PS-NPs and PS-NH_2-NPs compared to PS-COOH-NPs. These findings are in agreement with the previous study by Nolte et al. (2017), who investigated the influence of surface functional groups of polystyrene NPs on their adsorption to the cell surface of the alga *P. subcapitata*. It was found that PS-NPs and PS-NH_2-NPs have a higher affinity for binding to the algal cell wall than the negatively charged PS-COOH-NPs, which is attributed to electrostatic repulsion between the negatively charged PS-COOH-NPs and the negatively charged cell wall (Eslick et al., 2014; Lesniewska et al., 2024; Parkinson et al., 2022). Furthermore, the lower relative signal of PS-COOH-NPs in the cell-associated fraction compared to the two other types of polystyrene NPs, is consistent with results obtained for the alga *Chlorella sorokiniana*, where the authors reported lower uptake of PS-COOH-NPs compared to PS-NH_2-NPs (Xu et al., 2024). Based on these observations, functional groups appear to have an important impact on the aggregation of polystyrene NPs in water and their adhesion to cell surfaces, which in turn affects their phytotoxicity.

Exposure of green algae to polystyrene NPs has been associated with several adverse cellular effects, such as alterations in algal cell morphology, including cell enlargement and cell wall deformation in *C. vulgaris* (Hazeem et al., 2020) and *Phaeodactylum helgolandica* (Wang et al., 2020). Polystyrene NPs have also been found to promote cellular aggregation and cause structural disruption that impairs membrane integrity in *S. obliquus* (Wang et al., 2023) and *Chlorella pyrenoidosa* (Guo et al., 2025). Moreover, exposure of *Gymnodinium aeruginosum* to polystyrene NPs resulted in chloroplast degradation, starch depletion, cell wall thickening, and plasmolysis (Huang et al., 2021), which is consistent with the results of our study, in which plasmolysis and destabilization of the thylakoid membrane were observed in *C. vulgaris* treated with all types of polystyrene NPs, with the most pronounced changes occurring with non-functionalized particles.

Although some studies have shown that exposure of green algae to polystyrene NPs can increase ROS production (Hazeem et al., 2020; Natarajan et al., 2022; Xiang et al., 2023), our research suggests that this is not a general mechanism and depends on NP surface functionalization. Indeed, treatment with PS-NPs in *C. vulgaris* cells did not lead to an increase in ROS, either overall or in the form of H_2O_2, whereas both types of functionalized particles induced oxidative stress. PS-NH_2-NPs increased only H_2O_2 content, while PS-COOH-NPs significantly elevated all measured ROS parameters. In previous studies, exposure of *C. vulgaris* to PS-COOH-NPs (Hazeem et al., 2020) resulted in increased ROS formation, and similar results were observed after treatment of *Chlorella* and *Scenedesmus* with PS-NH_2-NPs and PS-COOH-NPs (Bhattacharya et al., 2010). Moreover, polystyrene NPs with functional groups caused higher ROS production in marine *Chlorella* sp. cells compared to PS-NPs without functional groups (Natarajan et al., 2020), which is consistent with our results. It is assumed that functionalized NPs have a greater potential for interactions between their functional groups and cell and mitochondrial membranes, leading to a higher ROS content in the cell (Płuciennik et al., 2024; Zhang et al., 2022).

Although non-functionalized PS-NPs did not stimulate detectable ROS and/or H_2O_2 production, they still caused significant damage to all biomolecules analyzed, likely due to direct membrane disruption, physical stress and possible earlier transient oxidative responses that were no longer detectable at the time of measurement (Bhattacharjee et al., 2014; Meng et al., 2023). This result could indicate that increased ROS production was triggered much earlier than 72 h after treatment, when the measurements were performed, and that these molecules had already been neutralized by the antioxidant machinery. However, to confirm such dynamics, additional measurements at multiple time points are needed. Sendra et al. (2019) showed that PS-NPs significantly stimulated ROS synthesis in *Phaeodactylum tricornutum* algal cells, but only within the first 24 h, while the measured values after 72 h were comparable to those of the control. In addition, it is possible that the cells did not have enough time to fully repair the damaged proteins, lipids, and DNA after neutralization of various ROS by the antioxidant machinery. Indeed, studies on the recovery time of the alga *Scenedesmus* sp. after induced oxidative stress have shown that the activity of certain metabolic enzymes returns to an optimal state only after 72 h (Tripathi et al., 2004), while a much longer recovery time has been found in several plant species (Chmielowska-Bąk and Deckert, 2021). Regarding the functionalized particles, PS-NH_2-NPs caused lipid peroxidation and genotoxic effects, while PS-COOH-NPs caused significant carbonylation of algal proteins in addition to DNA damage. These results indicate that treatments with both functionalized NPs induced oxidative stress in algal cells, but the effects depended on the individual properties of the NPs, including their surface functionalization and charge. Although both NPs with functional groups caused genotoxic effects, PS-NH_2-NPs damaged only lipids, while PS-COOH-NPs damaged only proteins. Due to their surface functionality and initial positive charge, PS-NH_2-NPs may interact more strongly with the cell envelope, which could facilitate their close cell association, as suggested by their higher relative signal in the cell-associated fraction. Such close interaction with the cell envelope has been proposed to enlarge existing pores and promote the formation of new ones, which in turn can cause degradation of

the membranes themselves (Dai et al., 2022). In contrast, PS-COOH-NPs showed a lower relative signal in the cell-associated fraction, possibly reflecting weaker retention after EPS removal and less pronounced close association with the cell envelope. Nevertheless, carboxylated surface functional groups may promote protein adsorption, contributing to protein impairment, as reflected by increased protein carbonylation (Kokkinopoulou et al., 2017; Panico et al., 2022). In addition, PS-COOH-NPs caused the most significant increase in ROS content in the cells, which may subsequently have an extremely negative effect on protein structure and activity (Li et al., 2022b).

Under oxidative stress, algae activate both enzymatic and non-enzymatic antioxidant mechanisms to reduce ROS levels (Yasur and Rani, 2013). In this study, all treatments modulated the antioxidant system in algal cells, consistent with previous research on algae treated with polystyrene NPs (Huang et al., 2021; Xiang et al., 2023; Zhao et al., 2020). Treatment with PS-NPs slightly increased PPX activity and significantly increased APX activity, which may indicate that peroxidases have sufficient capacity to remove H_2O_2. Since PS-NPs have been shown to increase ROS production in algae within the first 24 h (Sendra et al., 2019), it is possible that antioxidant enzyme activity increased significantly during this period and decreased later as ROS content declined. A recent study on the alga *S. obliquus* found that antioxidant enzymes are activated within 24 h after treatment with polystyrene MPs, with enzyme activity decreasing thereafter (Wang et al., 2023). After exposure to functionalized NPs, APX and PPX activities increased significantly after both PS-NH_2-NPs and PS-COOH-NPs treatments, indicating activation of peroxide-scavenging pathways and aligning with the observed increase in H_2O_2 content after these treatments compared to the control. In contrast, CAT activity showed a weaker and less consistent response, with no significant differences between functionalized NP treatments and the control, although the slight increase observed with PS-NH_2-NPs compared to the control was significant in comparison to PS-NPs. For SOD, a somewhat opposite effect was observed: the highest activity occurred with PS-NPs, although it was not significantly different from the control, whereas functionalized NPs caused a decrease in SOD activity, with PS-NH_2-NPs showing a significant decrease, possibly due to the interaction of amino functional groups with the SOD enzyme (He et al., 2020) or the induction of oxidative stress, which in turn inhibits SOD activity (Zhang et al., 2022). However, the absence of increased SOD activity and the induction of at least one of the peroxidases after all treatments suggest that peroxidases are among the main antioxidant enzymes involved in reducing oxidative stress caused by polystyrene NPs.

Analysis of the non-enzymatic antioxidants showed that each treatment led to a significant reduction in proline content. As polystyrene NPs have been shown to significantly affect algal metabolism, the decrease in proline content is possibly a consequence of increased energy demand under stress conditions, which can stimulate the breakdown of amino acids to generate additional energy (Ingrisano et al., 2023). Proline is one of the energy-rich amino acids whose degradation produces $FADH_2$ and NADH, which are further utilized in the mitochondria for energy production (Ingrisano et al., 2023). Therefore, the lower proline content after all treatments may be induced by the increased energy demand of the algal cells. In addition, all treatments caused a significant decrease in GSH in the algal cells compared to the control. As GSH is involved in the reduction of ROS content by oxidation to the GSSG form, the decrease in GSH in the cells could result from an activated antioxidant defense mechanism in the algae due to exposure to polystyrene NPs (Manke et al., 2013).

Overall, the results on the stability and cell association of polystyrene NPs and their influence on oxidative stress indicate that all tested NPs interacted with the EPS layer and remained associated with *C. vulgaris* cells after EPS removal, although most detectable polystyrene was retained in the EPS layer, suggesting its protective role (Bhattacharjee et al., 2014; Sendra et al., 2019). Notably, cell-associated retention was more pronounced in treatments with non-functionalized PS-NPs and amino-functionalized PS-NH_2-NPs, consistent with their more persistent positive surface charge and higher affinity for the negatively charged algal surface (Eslick et al., 2014; Zhang et al., 2022). This stronger cell association was accompanied by oxidative stress responses of varying intensities and profiles. PS-NH_2-NPs and PS-COOH-NPs induced a significant increase in ROS and/or H_2O_2 production, leading to oxidative DNA damage and, depending on NP surface functionalization, damage to lipids or proteins (Lin et al., 2025; Nolte et al., 2017; Zhang et al., 2022). Conversely, despite the absence of detectable increases in ROS at the 72 h time point, PS-NPs caused marked biomolecular damage, which may result from physical disruption of cellular membranes and/or earlier transient oxidative responses that were no longer detectable at the time of measurement (Bhattacharjee et al., 2014; Meng et al., 2023). All NP treatments triggered treatment-specific changes in antioxidant enzyme activities, characterized mainly by increased peroxidase activity and reduced SOD activity only after PS-NH_2-NP exposure, accompanied by depletion of non-enzymatic antioxidants such as proline and glutathione, suggesting disturbed redox homeostasis (Adhikari et al., 2025; Li et al., 2023b; Xiang et al., 2023). Importantly, these stress responses were not associated with a significant reduction in final cell density or specific growth rate, and the low proportion of PI-positive cells indicated no pronounced loss of cell membrane integrity. This suggests that the applied NP concentration induced primarily sublethal physiological stress rather than acute algicidal effects. These findings underscore that both the surface chemistry of NPs and their interactions with the EPS and algal surface strongly influence cell-associated retention and oxidative stress responses in *C. vulgaris*.

The exploratory PCA further supported this treatment-specific interpretation by integrating oxidative stress markers, biomolecular damage parameters, antioxidant responses and photosynthesis-related parameters into a single multivariate overview. Although PCA was not used as a confirmatory statistical test, the distribution of samples along the first two principal components was consistent with the patterns observed in the individual analyses. PS-NH_2-NPs shifted toward negative PC1 and PC2 values and were mainly associated with pigment-related variables, APX activity and lipid peroxidation, supporting the interpretation that amino-functionalized particles induced changes related to membrane damage and pigment-level adjustment. In contrast, PS-COOH-NPs were separated mainly along positive PC2 values and were more closely associated with ROS-related parameters, H_2O_2 accumulation, protein oxidation, DNA damage and increased PI_{abs}, supporting the interpretation that carboxyl-functionalized particles induced a response profile dominated by oxidative stress and protein impairment. Non-functionalized PS-NPs showed partial overlap with control samples in the PCA score plot, indicating that their overall multivariate response was less clearly separated than that of the functionalized particles, despite the significant biomolecular damage observed in the univariate analyses. Therefore, the PCA provided an integrated visualization of the distinct stress profiles induced by differently functionalized polystyrene NPs and was consistent with the conclusion that surface chemistry modulates the balance between oxidative stress, antioxidant defense and photosynthetic adjustment in *C. vulgaris*.

Furthermore, prior research on various algal species has demonstrated that polystyrene NPs cause a decrease in chlorophyll and carotenoid content (Hazeem et al., 2020; Wang et al., 2020; Xiang et al., 2023). In this study, only PS-NPs treatment significantly reduced the content of all analyzed photosynthetic pigments compared to the control. In contrast, PS-NH_2-NPs induced an overall increase in pigment content, although it was statistically significant only for carotenoids compared to the control, while for chl *a* it was significant compared to the two other treatments. PS-COOH-NPs did not cause significant changes in pigment content compared to the control. These findings are in agreement with previous research showing that PS-NPs without functional groups cause a greater decrease in chl *a* content than functionalized nanoparticles in the cells of the alga *C. vulgaris* (Hazeem et al.,

2020). PS-NPs have been shown to bind to the surface of algal cells, which can limit the amount of light available for photosynthesis and consequently contribute to reduced pigment content (Bhattacharya et al., 2010; Hazeem et al., 2020). The altered pigment content can influence metabolism and energy transfer in photochemical reactions, thereby contributing to photosynthetic impairment (Nguyen et al., 2020). However, the photosynthetic rate data indicate that pigment loss and probable shading alone cannot fully explain the observed responses, since all NP treatments reduced oxygen evolution at the growth light intensity, while the pigment and oxidative stress responses differed among treatments. This suggests that photosynthetic impairment resulted from multiple, treatment-specific processes, including altered light availability, oxidative stress, thylakoid disorganization, and possible changes in photosynthesis-related proteins. These results are consistent with a previous study showing that exposure of *Chlamydomonas reinhardtii* to PS-NPs decreases photosynthetic activity (Li et al., 2020).

Additionally, in our study all treatments increased the PI_{abs}, while none of them significantly altered the F_v/F_m when compared to the control sample. Our observations align with the findings of earlier research in which polystyrene NPs showed no significant effect on photosynthetic efficiency in algae (Sjollema et al., 2016; Wu et al., 2021). Since the F_v/F_m represents the maximum potential of PSII to convert light energy into chemical energy for electron transfer, our results indicate that treatments with all NPs had no significant effect on the efficiency of PSII photochemistry (Maxwell and Johnson, 2000). The additional JIP-test parameters further supported this interpretation. Exposure to PS-NH_2-NPs and PS-COOH-NPs significantly decreased ABS/RC and DI_0/RC, whereas ET_0/RC remained unchanged across all treatments. This indicates that functionalized polystyrene NPs decreased both energy absorption and dissipation, while electron transport per active PSII reaction center was largely preserved. Therefore, the reduced oxygen evolution observed at 80 photons μmol m^{-2} s^{-1}, corresponding to the growth light intensity, and at 120 μmol photons m^{-2} s^{-1}, was not accompanied by inhibition of primary PSII photochemistry. The decrease in oxygen evolution therefore cannot be attributed solely to impaired PSII photochemistry, as F_v/F_m, PI_{abs} and other measured JIP-parameters did not indicate downregulation of PSII. However, based on general knowledge of photosynthesis, several processes may have contributed to the reduced oxygen evolution rate. Oxygen-consuming processes closely related to photosynthesis under stressful conditions (Masojídek et al., 2021), such as photorespiration under limited CO_2 conditions, may be relevant in our study because measurements were performed in BBM medium without added bicarbonate. In addition, as surface-associated plastic NPs have been reported to hinder algal photosynthesis by physically blocking light and gas exchange, the retention of polystyrene NPs at the algal surface may limit CO_2 availability (Bhattacharya et al., 2010; Sun et al., 2024). Furthermore, chlororespiration and the Mehler reaction, which lead to oxygen reduction (Masojídek et al., 2021), may also contribute to the decreased oxygen evolution rate. Considering the functionality of PSII, previous studies on plants have reported that, under certain stress conditions, ascorbate and proline can serve as internal alternative electron donors to PSII. In addition, electrons recycled from downstream acceptors, such as the plastoquinone pool, back to PSII can donate electrons to PSII (De Ronde et al., 2004; Zhao et al., 2021). These processes could explain why ET_0/RC was not affected, but their actual contribution in our study could be a subject for further research. A previous study showed that polystyrene NPs with a diameter of 100 nm accumulate on the surface of *Microcystis aeruginosa* cells and cause changes in photosynthesis (Wu et al., 2021). The increased PI_{abs} after all treatments may therefore reflect an adjustment of the photosynthetic apparatus under NP-induced stress, potentially including decreased light availability, rather than a direct increase in photosynthetic efficiency (Galmés et al., 2013; Seemann, 1989).

Cell-free optical measurements showed limited light attenuation for PS-NPs and PS-NH_2-NPs, whereas PS-COOH-NPs showed a moderate increase after 72 h. However, these measurements reflect bulk NP suspensions and do not exclude localized shading at the algal surface. Because polystyrene NPs were retained in the EPS-associated and cell-associated fractions, local enrichment of particles around the algal envelope could have reduced light availability at the cell surface even when overall attenuation in the surrounding medium was low. Therefore, shading may have contributed partially to the observed photosynthetic impairment, particularly under conditions of local NP enrichment around algal cells, but it does not fully explain the treatment-specific oxidative stress, biomolecular damage and pigment or JIP response patterns.

The different responses to PS-NPs, PS-NH_2-NPs, and PS-COOH-NPs likely reflect a complex interplay of charge-mediated surface adhesion, membrane integrity, oxidative targeting, and adaptive biochemical responses (Zhang et al., 2022). PS-NPs induced a decrease in the content of chl *a*, chl *b* and carotenoids, which, together with the pronounced thylakoid alterations observed by TEM, suggests direct impairment of the light-harvesting system and thylakoid structure. This pigment decline is consistent with widespread findings that PS-NPs exposure reduces pigment content in green algae such as *C. pyrenoidosa*, *C. reihhardtii* and *S. obliquus*, impairing photosynthetic efficiency and growth (Cao et al., 2022; Li et al., 2021b). The reduction in pigment content likely reflects pigment degradation and changes in light utilization associated with NPs exposure, with reported pigment content depending on exposure duration and NPs properties (Cao et al., 2022; Guo et al., 2025). In contrast, despite a reduced photosynthetic rate and unchanged F_v/F_m values, PS-NH_2-NPs caused an overall upward trend in pigment content, with a significant increase observed only for carotenoids, suggesting a stress-related pigment adjustment rather than a uniform increase in all photosynthetic pigments. Similar responses have been observed in other species, where exposure to PS-NH_2-NPs elevated chlorophyll levels (Hanachi et al., 2022; Khoshnamvand et al., 2021). This adjustment of pigment levels may represent a stress-mediated adaptive response, aimed at supporting light capture under reduced photosynthetic activity or partial membrane damage. As for PS-COOH-NPs, pigment levels remained stable, with no change in chlorophyll or carotenoid content, indicating that chloroplast pigment synthesis and stability were largely preserved. However, the photosynthetic rate declined and PI_{abs} increased after PS-COOH-NPs exposure. The literature shows that PS-COOH-NPs often cause oxidative damage primarily targeting proteins rather than pigments (Kokkinopoulou et al., 2017; Panico et al., 2022; Zhang et al., 2022), which is consistent with our findings of protein and DNA oxidation. Moreover, possibly related to their surface formulation, PS-COOH-NPs showed the lowest relative cell-associated signal, suggesting weaker retention after EPS removal and a less pronounced close association with the algal envelope. Since pigment levels remained largely unchanged after PS-COOH-NP exposure, the observed photosynthetic impairment is unlikely to reflect direct inhibition of pigment synthesis. Instead, it may be influenced by oxidative stress-related changes and effects on photosynthesis-related proteins, as suggested by exploratory PCA, in which ROS-related parameters, H_2O_2 accumulation and protein carbonylation were closely associated in samples treated with PS-COOH-NPs.

Several limitations of this study should be considered when interpreting the results. The experiment was performed using a single, relatively high NP concentration and a 72 h endpoint; therefore, the findings should be viewed as a comparative high-exposure assessment of surface-functionalization-dependent response patterns rather than an environmentally realistic dose-response evaluation. Furthermore, this study used commercial particle suspensions. Although manufacturer documentation provided nominal surface formulations and partial information on suspension matrices and additives, quantitative functional group densities were not available. Therefore, the observed differences among NP types should be interpreted as responses to commercial surface formulations rather than attributed exclusively to isolated amino or

carboxyl functional groups. In addition, transient ROS responses at earlier exposure stages cannot be excluded because ROS and H_2O_2 were measured only at the final endpoint. Finally, the Py-GC-MS cell-associated fraction should be interpreted as evidence of cell-associated retention after EPS removal, not as direct confirmation of intracellular NP uptake, and PCA should be considered an exploratory multivariate visualization rather than a confirmatory statistical approach.

5. Conclusion

This research shows that the surface functionalization/formulation of polystyrene NPs plays an important role in modulating their interactions with *C. vulgaris* and the resulting phytotoxic effects. All NP types were stable in the culture medium and were retained in the EPS-associated and cell-associated fractions, and induced pronounced ultrastructural changes, including plasmolysis and thylakoid disorganization. It should be noted that the Py-GC-MS data were qualitative and relative/semi-quantitative, and that the cell-associated fraction does not provide direct evidence of intracellular NP uptake. Among the tested NPs, PS-COOH-NPs showed the lowest cell-associated retention, which may be related to differences in surface interactions with the algal cell envelope, but uniquely induced elevated ROS levels and protein oxidation. In contrast, PS-NPs showed pronounced EPS- and cell-associated retention and caused the most extensive biomolecular damage, while PS-NH_2-NPs triggered less severe biomolecular damage but activated selected antioxidant enzymes. Despite differences in response profiles, all polystyrene NPs decreased the photosynthetic rate, with stronger effects observed for both functionalized NPs at growth light intensity. Reduced light availability caused by particle-associated shading may have contributed to the observed decrease in photosynthetic rate, particularly under conditions of local NP enrichment around algal cells. However, shading alone is unlikely to fully explain the treatment-specific responses, particularly because the different NP types induced distinct oxidative stress, ultrastructural and some of photosynthetic endpoints. Overall, these findings underscore that nanoparticle surface functionalization strongly modulates their behavior, cell-association, and phytotoxic responses. However, these findings should be interpreted within the context of a single high-exposure concentration and a 72 h endpoint, which limits direct extrapolation to environmentally realistic scenarios. In addition, because commercial particle suspensions were used, the observed differences should not be attributed exclusively to isolated amino or carboxyl functional groups. Given the ecological importance of algae as primary producers, the results further emphasize that ecotoxicological evaluations of plastic NPs should consider the combined influence of surface properties, medium composition and other environmental factors that can strongly modulate NP interactions with algal cells.

CRediT authorship contribution statement

Bruno Komazec: Writing – review & editing, Writing – original draft, Visualization, Methodology, Investigation, Formal analysis, Conceptualization. **Biljana Balen:** Writing – review & editing, Project administration, Methodology. **Željka Vidaković-Cifrek:** Writing – review & editing, Methodology, Formal analysis. **Petra Cvjetko:** Methodology, Investigation, Formal analysis. **Nino Dimitrov:** Methodology, Investigation, Formal analysis. **Petra Peharec Štefanić:** Writing – review & editing, Writing – original draft, Visualization, Supervision, Methodology, Investigation, Conceptualization.

Funding sources

This work was funded by the Croatian Science Foundation, grant number HRZZ-IP-2022-10-3824, from the European Union's Horizon 2020 Research and Innovation Program under grant agreement No. 823717-ESTEEM3, and the research grant "Molecular basis of abiotic stress in plants" of the Faculty of Science, University of Zagreb, Croatia.

Declaration of competing interest

The authors declare that they have no known competing financial interests or personal relationships that could have appeared to influence the work reported in this paper.

Appendix A. Supplementary data

Supplementary data to this article can be found online at https://doi.org/10.1016/j.plaphy.2026.111698.

Data availability

Data will be made available on request.

References

Adhikari, A., Balhara, R., Hossain, Z., Singh, K., 2025. Mechanistic insights into polystyrene nanoplastics (PSNPs) mediated imbalance of redox homeostasis and disruption of antioxidant defense system leading to oxidative stress in black mustard (*Brassica nigra* L.). Plant Physiol. Biochem. 229, 110480.

Aebi, H., 1984. Catalase in vitro. In: Methods Enzymol, pp. 121–126.

Alimi, O.S., Farner Budarz, J., Hernandez, L.M., Tufenkji, N., 2018. Microplastics and nanoplastics in aquatic environments: aggregation, deposition, and enhanced contaminant transport. Environ. Sci. Technol. 52, 1704–1724.

Aly, S.M., ElBanna, N.I., Fathi, M., 2024. Chlorella in aquaculture: challenges, opportunities, and disease prevention for sustainable development. Aquac. Int. 32, 1559–1586.

Awet, T.T., Kohl, Y., Meier, F., Straskraba, S., Grün, A.L., Ruf, T., et al., 2018. Effects of polystyrene nanoparticles on the microbiota and functional diversity of enzymes in soil. Environ. Sci. Eur. 30, 11.

Babiak, W., Krzemińska, I., 2021. Extracellular polymeric substances (EPS) as microalgal bioproducts: a review of factors affecting EPS synthesis and application in flocculation processes. Energies 14, 4007.

Banerjee, A., Billey, L.O., McGarvey, A.M., Shelver, W.L., 2022. Effects of polystyrene micro/nanoplastics on liver cells based on particle size, surface functionalization, concentration and exposure period. Sci. Total Environ. 836, 155621.

Bates, L.S., Waldren, R.P., Teare, I.D., 1973. Rapid determination of free proline for water-stress studies. Plant Soil 39, 205–207.

Beauchamp, C., Fridovich, I., 1971. Superoxide dismutase: improved assays and an assay applicable to acrylamide gels. Anal. Biochem. 44, 276–287.

Bhattacharjee, S., Ershov, D., Islam, M.A., Kämpfer, A.M., Maslowska, K.A., van der Gucht, J., et al., 2014. Role of membrane disturbance and oxidative stress in the mode of action underlying the toxicity of differently charged polystyrene nanoparticles. RSC Adv. 4, 19321–19330.

Bhattacharya, P., Lin, S., Turner, J.P., Ke, P.C., 2010. Physical adsorption of charged plastic nanoparticles affects algal photosynthesis. J. Phys. Chem. C 114, 16556–16561.

Biba, R., Cvjetko, P., Jakopčić, M., Komazec, B., Tkalec, M., Dimitrov, N., et al., 2023. Phytotoxic effects of polystyrene and polymethyl methacrylate microplastics on *Allium cepa* roots. Plants 12, 747.

Bischoff, H.W., Bold, H.C., 1963. Some soil algae from enchanted rock and related algal species. Phycol. Stud. 4, 95.

Bradford, M.M., 1976. A rapid and sensitive method for the quantitation of microgram quantities of protein utilizing the principle of protein-dye binding. Anal. Biochem. 72, 248–254.

Cao, Q., Sun, W., Yang, T., Zhu, Z., Jiang, Y., Hu, W., et al., 2022. The toxic effects of polystyrene microplastics on freshwater algae *Chlorella pyrenoidosa* depends on the different size of polystyrene microplastics. Chemosphere 308, 136135.

Chae, Y., Kim, D., Kim, S.W., An, Y.J., 2018. Trophic transfer and individual impact of nano-sized polystyrene in a four-species freshwater food chain. Sci. Rep. 8, 284.

Chmielowska-Bąk, J., Deckert, J., 2021. Plant recovery after metal stress – a review. Plants 10, 450.

Cortés, C., Domenech, J., Salazar, M., Pastor, S., Marcos, R., Hernández, A., 2020. Nanoplastics as a potential environmental health factor: effects of polystyrene nanoparticles on human intestinal epithelial Caco-2 cells. Environ. Sci. Nano 7, 272–285.

Dai, S., Ye, R., Huang, J., Wang, B., Xie, Z., Ou, X., et al., 2022. Distinct lipid membrane interaction and uptake of differentially charged nanoplastics in bacteria. J. Nanobiotechnol. 20, 191.

de Abreu, F.C.P., da Costa, P.N.M., Brondi, A.M., Pilau, E.J., Gozzo, F.C., Eberlin, M.N., et al., 2014. Effects of cadmium and copper biosorption on *Chlorella vulgaris*. Bull. Environ. Contam. Toxicol. 93, 405–409.

De Ronde, J.A., Cress, W.A., Krüger, G.H.J., Strasser, R.J., Van Staden, J., 2004. Photosynthetic response of transgenic soybean plants, containing an Arabidopsis P5CR gene, during heat and drought stress. J. Plant Physiol. 161, 1211–1224.

Dere, Ş., Güneş, T., Sivaci, R., 1998. Spectrophotometric determination of chlorophyll - a, B and total carotenoid contents of some algae species using different solvents. Turk. J. Bot. 22, 13–18.
Dokl, M., Copot, A., Krajnc, D., Van Fan, Y., Vujanović, A., Aviso, K.B., et al., 2024. Global projections of plastic use, end-of-life fate and potential changes in consumption, reduction, recycling and replacement with bioplastics to 2050. Sustain. Prod. Consum. 51, 498–518.
Eslick, E.M., Beilby, M.J., Moon, A.R., 2014. A study of the native cell wall structures of the marine alga *Ventricaria ventricosa* (Siphonocladales, Chlorophyceae) using atomic force microscopy. Microscopy 63, 131–140.
Field, C.B., Behrenfeld, M.J., Randerson, J.T., Falkowski, P., 1998. Primary production of the biosphere: integrating terrestrial and oceanic components. Science 281, 237–240.
Galmés, J., Aranjuelo, I., Medrano, H., Flexas, J., 2013. Variation in rubisco content and activity under variable climatic factors. Photosynth. Res. 117, 73–90.
Gayathri, V., Khan, T., Gowtham, M., Balan, R., Sebaey, T.A., 2025. Functionalized conductive polymer composites for tissue engineering and biomedical applications – a mini review. Front. Bioeng. Biotechnol. 13, 1533944.
Giri, S., Mukherjee, A., 2021. Ageing with algal EPS reduces the toxic effects of polystyrene nanoplastics in freshwater microalgae *Scenedesmus obliquus*. J. Environ. Chem. Eng. 9, 105978.
Gopalakrishnan, K., Kashian, D.R., 2022. Extracellular polymeric substances in green alga facilitate microplastic deposition. Chemosphere 286, 131814.
Guo, Z., Chen, T., Wang, M., Qin, M., 2025. Size-dependent effects of polystyrene nanoplastics on freshwater microalgae after long-term exposure. Water 17, 655.
Gyori, B.M., Venkatachalam, G., Thiagarajan, P.S., Hsu, D., Clement, M.V., 2014. OpenComet: an automated tool for comet assay image analysis. Redox Biol. 2, 457–465.
Hadiyanto, H., Khoironi, A., Dianratri, I., Joelyna, F.A., Christwardana, M., Sabhira, A.I., et al., 2025. Microplastic removal in aquatic systems using extracellular polymeric substances (EPS) of microalgae. Sustain. Environ. 11, 2454756.
Hanachi, P., Khoshnamvand, M., Walker, T.R., Hamidian, A.H., 2022. Nano-sized polystyrene plastics toxicity to microalgae *Chlorella vulgaris*: toxicity mitigation using humic acid. Aquat. Toxicol. 245, 106123.
Hazeem, L.J., Yesilay, G., Bououdina, M., Perna, S., Cetin, D., Suludere, Z., et al., 2020. Investigation of the toxic effects of different polystyrene micro-and nanoplastics on microalgae *Chlorella vulgaris* by analysis of cell viability, pigment content, oxidative stress and ultrastructural changes. Mar. Pollut. Bull. 156, 111278.
He, Y., Li, J., Chen, J., Miao, X., Li, G., He, Q., et al., 2020. Cytotoxic effects of polystyrene nanoplastics with different surface functionalization on human HepG2 cells. Sci. Total Environ. 723, 138180.
Heath, R.L., Packer, L., 1968. Photoperoxidation in isolated chloroplasts. Arch. Biochem. Biophys. 125, 189–198.
Huang, W., Zhao, T., Zhu, X., Ni, Z., Guo, X., Tan, L., et al., 2021. The effects and mechanisms of polystyrene and polymethyl methacrylate with different sizes and concentrations on *Gymnodinium aeruginosum*. Environ. Pollut. 287, 117626.
Hund-Rinke, K., Sinram, T., Schlich, K., Nickel, C., Dickehut, H.P., Schmidt, M., et al., 2020. Attachment efficiency of nanomaterials to algae as an important criterion for ecotoxicity and grouping. Nanomaterials 10, 1021.
Ingrisano, R., Tosato, E., Trost, P., Gurrieri, L., Sparla, F., 2023. Proline, cysteine and branched-chain amino acids in abiotic stress response of land plants and microalgae. Plants 12, 3410.
Jachimowicz, P., Babkiewicz, E., Gavlova, A., Lang, J., Mądzielewska, W.I., Maszczyk, P., et al., 2026. Global microplastic contamination in freshwater lakes: spatial patterns, environmental drivers, and methodological challenges. Environ. Res. 291, 123585.
Jeffrey, S.W., Humphrey, G.F., 1975. New spectrophotometric equations for determining chlorophylls a, b, c1 and c2 in higher plants, algae and natural phytoplankton. Biochem. Physiol. Pflanz. 167, 191–194.
Jiang, J., Thayumanavan, S., 2005. Synthesis and characterization of amine-functionalized polystyrene nanoparticles. Macromolecules 38, 5886–5891.
Jin, Y., Lei, Z., Taynton, P., Huang, S., Zhang, W., 2019. Malleable and recyclable thermosets: the next generation of plastics. Matter 1, 1456–1493.
Kaur, M., Saini, K.C., Ojah, H., Sahoo, R., Gupta, K., Kumar, A., et al., 2022. Abiotic stress in algae: response, signaling and transgenic approaches. J. Appl. Phycol. 34, 1843–1869.
Khatiwada, J.R., Madsen, C., Warwick, C., Shrestha, S., Chio, C., Qin, W., 2023. Interaction between polyethylene terephthalate (PET) microplastic and microalgae (*Scenedesmus spp.*): effect on the growth, chlorophyll content, and hetero-aggregation. Environ. Adv. 13, 100399.
Khoshnamvand, M., Hanachi, P., Ashtiani, S., Walker, T.R., 2021. Toxic effects of polystyrene nanoplastics on microalgae *Chlorella vulgaris*: changes in biomass, photosynthetic pigments and morphology. Chemosphere 280, 130725.
Khoshnamvand, M., You, D., Xie, Y., Feng, Y., Sultan, M., Pei, D.S., et al., 2024a. Alleviating binary toxicity of polystyrene nanoplastics and atrazine to *Chlorella vulgaris* through humic acid interaction: Long-term toxicity using environmentally relevant concentrations. Chemosphere 358, 142111.
Khoshnamvand, M., You, D., Xie, Y., Feng, Y., Sultan, M., Wei, X., et al., 2024b. Presence of humic acid in the environment holds promise as a potential mitigating factor for the joint toxicity of polystyrene nanoplastics and herbicide atrazine to *Chlorella vulgaris*: 96-h acute toxicity. Chemosphere 357, 142061.
Kokkinopoulou, M., Simon, J., Landfester, K., Mailänder, V., Lieberwirth, I., 2017. Visualization of the protein corona: towards a biomolecular understanding of nanoparticle-cell-interactions. Nanoscale 9, 8858–8870.
Komazec, B., Cvjetko, P., Balen, B., Letofsky-Papst, I., Lyons, D.M., Peharec Štefanić, P., 2023. The occurrence of oxidative stress induced by silver nanoparticles in *Chlorella vulgaris* depends on the surface-stabilizing agent. Nanomaterials 13, 1967.
Komazec, B., Vitko, S., Balen, B., Cindrić, M., Biba, R., Peharec Štefanić, P., 2025. Multi-parameter analysis of photosynthetic and molecular responses in *Chlorella vulgaris* exposed to silver nanoparticles and ions. Toxics 13, 627.
Le Juge, C., Grassl, B., Allan, I.J., Gigault, J., 2023. Identification of polystyrene nanoplastics from natural organic matter in complex environmental matrices by pyrolysis–gas chromatography–mass spectrometry. Anal. Bioanal. Chem. 415, 2999–3006.
Lesniewska, N., Duval, J.F.L., Caillet, C., Razafitianamaharavo, A., Pinheiro, J.P., Bihannic, I., et al., 2024. Physicochemical surface properties of *Chlorella vulgaris*: a multiscale assessment, from electrokinetic and proton uptake descriptors to intermolecular adhesion forces. Nanoscale 16, 5149–5163.
Li, B.B., Zhang, S.B., Lv, Y.Y., Wei, S., Hu, Y.S., 2022b. Reactive oxygen species-induced protein carbonylation promotes deterioration of physiological activity of wheat seeds. PLoS One 17, e0263553.
Li, C., Gao, Y., He, S., Chi, H.Y., Li, Z.C., Zhou, X.X., et al., 2021a. Quantification of nanoplastic uptake in cucumber plants by pyrolysis gas chromatography/mass spectrometry. Environ. Sci. Technol. Lett. 8, 633–638.
Li, R., Wang, B., Nan, F., Lv, J., Liu, X., Liu, Q., et al., 2023b. Effects of polystyrene nanoplastics on the physiological and biochemical characteristics of microalga *Scenedesmus quadricauda*. Environ. Pollut. 319, 120987.
Li, S., Wang, P., Zhang, C., Zhou, X., Yin, Z., Hu, T., et al., 2020. Influence of polystyrene microplastics on the growth, photosynthetic efficiency and aggregation of freshwater microalgae *Chlamydomonas reinhardtii*. Sci. Total Environ. 714, 136767.
Li, X., Ji, S., He, E., Peijnenburg, W.J.G.M., Cao, X., Zhao, L., et al., 2022a. UV/ozone induced physicochemical transformations of polystyrene nanoparticles and their aggregation tendency and kinetics with natural organic matter in aqueous systems. J. Hazard Mater. 433, 128790.
Li, Y., Liu, S., Ji, Z., Sun, J., Liu, X., 2023a. Distinct responses of *Chlorella vulgaris* upon combined exposure to microplastics and bivalent zinc. J. Hazard Mater. 442, 130137.
Li, Y., Liu, X., Shinde, S., Wang, J., Zhang, P., 2021b. Impacts of micro- and nanoplastics on photosynthesis activities of photoautotrophs: a mini-review. Front. Microbiol. 12, 773226.
Lin, W., Jiang, R., Hu, S., Xiao, X., Wu, J., Wei, S., et al., 2019. Investigating the toxicities of different functionalized polystyrene nanoplastics on *Daphnia magna*. Ecotoxicol. Environ. Saf. 180, 509–516.
Lin, Z., Xu, D., Zhao, Y., Sheng, B., Wu, Z., Wen, X., et al., 2025. Micro/nanoplastics in plantation agricultural products: behavior process, phytotoxicity under biotic and abiotic stresses, and controlling strategies. J. Nanobiotechnol. 23, 231.
Liu, X., Jiang, X., Li, A., 2025. Bio-entrapment of *Chlorella vulgaris* mimicking granular sludge: insights into aggregated microalgae growth and symbiotic bacteria under antibiotic stress. Chem. Eng. J. 514, 163075.
Loos, C., Syrovets, T., Musyanovych, A., Mailänder, V., Landfester, K., Nienhaus, G.U., et al., 2014. Functionalized polystyrene nanoparticles as a platform for studying bio–nano interactions. Beilstein J. Nanotechnol. 5, 2403–2412.
Manke, A., Wang, L., Rojanasakul, Y., 2013. Mechanisms of nanoparticle-induced oxidative stress and toxicity. Biomed Res. Int. 2013, 1–15.
Masojídek, J., Ranglová, K., Lakatos, G.E., Silva Benavides, A.M., Torzillo, G., 2021. Variables governing photosynthesis and growth in microalgae mass cultures. Processes 9, 820.
Mátai, A., 2017. É. Hideg, A comparison of colorimetric assays detecting hydrogen peroxide in leaf extracts. Anal. Methods 9, 2357–2360.
Maxwell, K., Johnson, G.N., 2000. Chlorophyll fluorescence – a practical guide. J. Exp. Bot. 51, 659–668.
Meng, Z., Stoll, S., Liu, W., 2023. Transformations, interactions, and acute biological responses of nanoplastics on mixotrophic microalgae *Poterioochromonas malhamensis*. Environ. Sci. Nano 10, 2459–2472.
Nakano, Y., Asada, K., 1981. Hydrogen peroxide is scavenged by ascorbate-specific peroxidase in spinach chloroplasts. Plant Cell Physiol. 22, 867–880.
Natarajan, L., Omer, S., Jetly, N., Jenifer, M.A., Chandrasekaran, N., Suraishkumar, G.K., et al., 2020. Eco-corona formation lessens the toxic effects of polystyrene nanoplastics towards marine microalgae *Chlorella sp*. Environ. Res. 188, 109842.
Natarajan, L., Soupam, D., Dey, S., Chandrasekaran, N., Kundu, R., Paul, S., et al., 2022. Toxicity of polystyrene microplastics in freshwater algae *Scenedesmus obliquus*: effects of particle size and surface charge. Toxicol. Rep. 9, 1953–1961.
Nayanathara Thathsarani Pilapitiya, P.G.C., Ratnayake, A.S., 2024. The world of plastic waste: a review. Clean. Mater. 11, 100220.
Ng, N.S., Ooi, L., 2021. A simple microplate assay for reactive oxygen species generation and rapid cellular protein normalization. Bio. Protoc. 11, 1–10.
Nguyen, M.K., Moon, J.Y., Lee, Y.C., 2020. Microalgal ecotoxicity of nanoparticles: an updated review. Ecotoxicol. Environ. Saf. 201, 110781.
Nolte, T.M., Hartmann, N.B., Kleijn, J.M., Garnæs, J., van de Meent, D., Jan Hendriks, A., et al., 2017. The toxicity of plastic nanoparticles to green algae as influenced by surface modification, medium hardness and cellular adsorption. Aquat. Toxicol. 183, 11–20.
OECD, 2022. Global Plastics Outlook: Economic Drivers, Environmental Impacts and Policy Options. OECD Publishing, Paris.
OECD, 2026. Test No. 201: freshwater alga and Cyanobacteria, growth inhibition test. In: OECD Guidelines for the Testing of Chemicals, Section, vol. 2. OECD Publishing, Paris.
Okoffo, E.D., Thomas, K.V., 2024. Mass quantification of nanoplastics at wastewater treatment plants by pyrolysis-gas chromatography-mass spectrometry. Water Res. 254, 121397.
Panico, S., Capolla, S., Bozzer, S., Toffoli, G., Dal Bo, M., Macor, P., 2022. Biological features of nanoparticles: protein corona formation and interaction with the immune system. Pharmaceutics 14, 2605.

Parkinson, S.J., Tungsirisurp, S., Joshi, C., Richmond, B.L., Gifford, M.L., Sikder, A., et al., 2022. Polymer nanoparticles pass the plant interface. Nat. Commun. 13, 7385.
Parsai, T., Figueiredo, N., Dalvi, V., Martins, M., Malik, A., Kumar, A., 2022. Implication of microplastic toxicity on functioning of microalgae in aquatic system. Environ. Pollut. 308, 119626.
Płuciennik, K., Sicińska, P., Misztal, W., Bukowska, B., 2024. Important factors affecting induction of cell death, oxidative stress and DNA damage by nano- and microplastic particles in vitro. Cells 13, 768.
Pradel, A., Ferreres, S., Veclin, C., El Hadri, H., Gautier, M., Grassl, B., et al., 2021. Stabilization of fragmental polystyrene nanoplastic by natural organic matter: insight into mechanisms. ACS ES&T Water 1, 1198–1208.
Salbitani, G., Bottone, C., Carfagna, S., 2017. Determination of reduced and total glutathione content in extremophilic microalga *Galdieria phlegrea*. Bio. Protoc. 7, 2–6.
Saxena, P., Saharan, V., Baroliya, P.K., Gour, V.S., Rai, M.K., Harish, 2021. Mechanism of nanotoxicity in *Chlorella vulgaris* exposed to zinc and iron oxide. Toxicol. Rep. 8, 724–731.
Seemann, J.R., 1989. Light adaptation/acclimation of photosynthesis and the regulation of ribulose-1, 5-bisphosphate carboxylase activity in sun and shade plants. Plant Physiol. 91, 379–386.
Sendra, M., Staffieri, E., Yeste, M.P., Moreno-Garrido, I., Gatica, J.M., Corsi, I., et al., 2019. Are the primary characteristics of polystyrene nanoplastics responsible for toxicity and ad/absorption in the marine diatom *Phaeodactylum tricornutum*? Environ. Pollut. 249, 610–619.
Sjollema, S.B., Redondo-Hasselerharm, P., Leslie, H.A., Kraak, M.H.S., Vethaak, A.D., 2016. Do plastic particles affect microalgal photosynthesis and growth? Aquat. Toxicol. 170, 259–261.
Sun, X.D., Yuan, X.Z., Jia, Y., Feng, L.J., Zhu, F.P., Dong, S.S., et al., 2020. Differentially charged nanoplastics demonstrate distinct accumulation in *Arabidopsis thaliana*. Nat. Nanotechnol. 15, 755–760.
Sun, Z., Zhang, S., Zheng, T., He, C., Xu, J., Lin, D., et al., 2024. Nanoplastics inhibit carbon fixation in algae: the effect of aging. Heliyon 10, e29814.
Tallec, K., Blard, O., González-Fernández, C., Brotons, G., Berchel, M., Soudant, P., et al., 2019. Surface functionalization determines behavior of nanoplastic solutions in model aquatic environments. Chemosphere 225, 639–646.
Taudul, B., Tielens, F., Calatayud, M., 2024. Raman characterization of plastics: a DFT study of polystyrene. J. Phys. Chem. B 128, 4243–4254.
Taylor, S.E., Pearce, C.I., Sanguinet, K.A., Hu, D., Chrisler, W.B., Kim, Y.M., et al., 2020. Polystyrene nano- and microplastic accumulation at Arabidopsis and wheat root cap cells, but no evidence for uptake into roots. Environ. Sci. Nano 7, 1942–1953.
Tripathi, B.N., Mehta, S.K., Gaur, J.P., 2004. Recovery of uptake and assimilation of nitrate in *Scenedesmus sp.* previously exposed to elevated levels of Cu^{2+} and Zn^{2+}. J. Plant Physiol. 161, 543–549.
Turan, N.B., Erkan, H.S., Engin, G.O., Bilgili, M.S., 2019. Nanoparticles in the aquatic environment: usage, properties, transformation and toxicity – a review. Process Saf. Environ. Prot. 130, 238–249.
Velev, O.D., Kaler, E.W., 1999. In situ assembly of colloidal particles into miniaturized biosensors. Langmuir 15, 3693–3698.
Wang, S., Liu, M., Wang, J., Huang, J., Wang, J., 2020. Polystyrene nanoplastics cause growth inhibition, morphological damage and physiological disturbance in the marine microalga *Platymonas helgolandica*. Mar. Pollut. Bull. 158, 111403.
Wang, W., Liu, H., Liu, H., Chen, J., Xu, X., Xia, J., et al., 2023. Effects of polystyrene microparticles on growth and physiological metabolism of microalgae *Scenedesmus obliquus*. Sustainability 15, 11223.
Wu, D., Wang, T., Wang, J., Jiang, L., Yin, Y., Guo, H., 2021. Size-dependent toxic effects of polystyrene microplastic exposure on *Microcystis aeruginosa* growth and microcystin production. Sci. Total Environ. 761, 143265.
Xiang, Q., Zhou, Y., Tan, C., 2023. Toxicity effects of polystyrene nanoplastics with different sizes on freshwater microalgae *Chlorella vulgaris*. Molecules 28, 3958.
Xu, M., Zhu, F., Yang, Y., Liu, M., Li, X., Jiang, Y., et al., 2024. Mechanism of transport and toxicity response of *Chlorella sorokiniana* to polystyrene nanoplastics. Ecotoxicol. Environ. Saf. 270, 115901.
Yang, W., Gao, P., Ye, Z., Chen, F., Zhu, L., 2024. Micro/nano-plastics and microalgae in aquatic environment: influence factor, interaction, and molecular mechanisms. Sci. Total Environ. 934, 173218.
Yasur, J., Rani, P.U., 2013. Environmental effects of nanosilver: impact on Castor seed germination, seedling growth, and plant physiology. Environ. Sci. Pollut. Res. 20, 8636–8648.
Yu, S., Shen, M., Li, S., Fu, Y., Zhang, D., Liu, H., et al., 2019. Aggregation kinetics of different surface-modified polystyrene nanoparticles in monovalent and divalent electrolytes. Environ. Pollut. 255, 113302.
Zhang, F., Wang, Z., Wang, S., Fang, H., Wang, D., 2019. Aquatic behavior and toxicity of polystyrene nanoplastic particles with different functional groups: complex roles of pH, dissolved organic carbon and divalent cations. Chemosphere 228, 195–203.
Zhang, H., Cheng, H., Wang, Y., Duan, Z., Cui, W., Shi, Y., et al., 2022. Influence of functional group modification on the toxicity of nanoplastics. Front. Mar. Sci. 8, 800782.
Zhao, T., Tan, L., Huang, W., Wang, J., 2019. The interactions between micro polyvinyl chloride (mPVC) and marine dinoflagellate *Karenia mikimotoi*: the inhibition of growth, chlorophyll and photosynthetic efficiency. Environ. Pollut. 247, 883–889.
Zhao, T., Tan, L., Zhu, X., Huang, W., Wang, J., 2020. Size-dependent oxidative stress effect of nano/micro-scaled polystyrene on *Karenia mikimotoi*. Mar. Pollut. Bull. 154, 111074.
Zhao, W., Ma, H., Gao, Z., Li, D., Lin, Y., Wu, C., et al., 2024. Uncovering the toxic effects and adaptive mechanisms of aminated polystyrene nanoplastics on microbes in sludge anaerobic digestion system: insight from extracellular to intracellular. J. Hazard Mater. 480, 136163.
Zhao, W., Zhang, Q.S., Tan, Y., Liu, Z., Ma, M.Y., Wang, M.X., et al., 2021. Photoprotective roles of ascorbate and PSII cyclic electron flow in the response of the seagrass *Zostera marina* to oxygen-evolving complex photoinactivation. Photosynthetica 59, 600–605.